Piezo1–Pannexin1 complex couples force detection to ATP secretion in cholangiocytes

Angélique Desplat, Virginie Penalba, Emeline Gros, Thibaud Parpaite, Bertrand Coste, Patrick Delmas

Piezo1-Pannexin 1 complex couples force detection to ATP secretion in cholangiocytes

Angélique Desplat[1], Virginie Penalba[1], Emeline Gros[1], Thibaud Parpaite[1], Bertrand Coste[1], Patrick Delmas[1]*

[1]Aix-Marseille-Université, CNRS, Laboratoire de Neurosciences Cognitives, UMR 7291, CS80011, Bd Pierre Dramard, 13344 Marseille, France.

*To whom correspondence may be addressed. Email patrick.delmas@univ-amu.fr

Phone: +33 4 91 69 89 78

Summary

Cholangiocytes actively contribute to the final composition of secreted bile. These cells are exposed to abnormal mechanical stimuli during obstructive cholestasis, which has a deep impact on their function. However, the effects of mechanical insults on cholangiocyte function are not understood. Combining gene silencing and pharmacological assays with live calcium imaging, we probed molecular candidates essential for coupling mechanical force to ATP secretion in mouse cholangiocytes. We show that Piezo1 and Pannexin1 are necessary for eliciting the downstream effects of mechanical stress. By mediating a rise in intracellular Ca^{2+}, Piezo1 acts as a mechanosensor responsible for translating cell swelling into activation of Panx1, which triggers ATP release and subsequent signal amplification through P2X4R. Co-immunoprecipitation and pull-down assays indicated physical interaction between Piezo1 and Panx1, which leads to stable plasma membrane complexes. Piezo1-Panx1-P2X4R ATP release pathway could be reconstituted in HEK Piezo1 KO cells. Thus, our data suggest that Piezo1 and Panx1 can form a functional signaling complex that controls force-induced ATP secretion in cholangiocytes. These findings may foster the development of novel therapeutic strategies for biliary diseases.

Keywords: liver; biliary diseases; biliary acids; mechanosensation; osmosensation

Introduction

Cholangiocytes are epithelial cells that line the intra-hepatic ducts of the biliary tree and serve important functions in bile formation. These cells modify the composition of primary hepatocyte-derived bile through a sequence of secretory and reabsorptive processes, critical for digestion and absorption of aliments (Banales et al., 2019). Although they account for a minor subset of the total hepatic cell population, they generate up to ≈40% of the bile volume formation (Boyer, 2013).

Cholangiocyte functions are regulated by multiple chemical factors, including hormones, peptides, nucleotides and bile acids, through a variety of intracellular signaling pathways, ion channels, transporters and receptors (Tabibian et al., 2013). Besides being targets for chemical mediators, cholangiocytes are also exposed to mechanical forces, including osmotic pressure and shear stress due to changes in bile composition and flow. Pathological conditions, associated with biliary obstruction, are also responsible for abnormal mechanical tension applied onto cholangiocyte plasma membrane. Primary sclerosing cholangitis (PSC) is an exemplar case, where fibroobliteration of the bile ducts is responsible for liver cirrhosis (Pinzani and Luong, 2018). Biliary outflow obstruction leads to increased biliary pressure, triggering pressure-induced maladaptative signaling in cholangiocytes that strengthens the disease progression (Maroni et al., 2015).

Mechanosensitive signaling has therefore emerged as a regulatory mechanism for the functions of cholangiocytes in both health and disease. However, the initiating steps translating mechanical forces into biochemical messages are not quite understood. Previous *in vitro* studies have demonstrated that mechanical strain and shear stress

induce an elevation of intracellular Ca^{2+} concentration ($[Ca^{2+}]_i$) through an increase in plasma membrane permeability to Ca^{2+} ions. These responses were proposed to depend on the primary cilium (Masyuk et al., 2008; Larusso and Masyuk, 2011; Mansini et al., 2018). Primary cilium's ability to integrate mechanical signals relies on the presence of a variety of ciliary-associated proteins that act as mechanotransducers. Among the various known mechanosensitive proteins, the importance of transient receptor potential (TRP) channels has been extensively studied. Changes in bile flow has been proposed to activate a ciliary complex formed by the association of TRPP1 (polycystin-1) and TRPP2 (polycystin-2) (Masyuk et al., 2006), two members of the TRPP (polycystin) protein family thought to hold mechanosensory properties (Nauli et al., 2003). On the other hand, the cilia-associated TRPV4 channel, a well-established osmosensor (Liedtke, 2005), has been shown to transduce changes in bile tonicity in cholangiocytes (Gradilone et al., 2007). Activation of these mechanosensitive channels promotes ATP release, which in turn, through autocrine/paracrine stimulation of one or more purinergic receptors, further increases $[Ca^{2+}]_i$ (Feranchak and Fitz, 2002). Purinergic signals promote transepithelial secretion of anions, water and HCO_3^- resulting in dilution and alkalinization of bile (Roman et al.,1999; Tabibian et al., 2013).

From the existing data has therefore emerged a model in which mechanotransducers coordinate ductal bile modification through intracellular Ca^{2+} signaling pathways and ATP release. However, neither the mechanotransducer apparatus, nor the ATP-release pathway has been definitely identified. Accordingly, the present study aims at dissecting the molecular mechanisms that couple mechanosensitive transducers to ATP secretion in cholangiocytes from mouse liver. We found that cholangiocytes from intrahepatic bile duct units (IBDUs) sense mechanical strain through the activation of

Piezo1, a Ca^{2+} permeable cation channel directly gated by mechanical forces (Coste et al., 2010; Ranade et al., 2015; Parpaite and Coste et al., 2017). The ensuing ATP release requires Pannexin-1 (Panx-1), a member of 'gap junction' protein family that forms non-junctional membrane channels permeable to ATP (Dahl, 2015; Taruno, 2018). Both proteins show potential for physical interaction. Thus, Piezo1 and Panx1 constitute a novel pathway to sense and signal mechanical cues in cholangiocytes. These proteins may be important new targets to regulate bile secretion in the treatment of cholestatic liver diseases.

Results

Isolated IBDU cells express cholangiocyte-specific markers

Primary cultures of cholangiocytes were made from mouse IBDUs. Quantitation of the proportion of cells expressing the cholangiocyte-specific marker cytokeratin 9 (CK19) revealed that ~80% of IBDU cells were positive for this maker at Day 5 in Vitro (DIV5) and DIV8, indicating an enriched population of intrahepatic cholangiocytes (**Supplemental Fig.1A,B**). Mouse cholangiocytes showed typical polygonal body shape with relatively regular dimensions (Tabibian et al., 2013). The absence of hepatocytes was demonstrated by the lack of staining for albumin, an hepatocyte-specific marker (≤1/1000 cells; **Supplemental Fig. 1A**). Other cholangiocyte specific markers, including cytokeratin 7 (CK7), the Cystic Fibrosis Transmembrane conductance Regulator (CFTR), the anion exchanger 2 (AE2) and the apical sodium-dependent bile acid transporter (ASBT) were also detected using RT-PCR (**Supplemental Fig.1C**).

Hypotonic stress increases membrane permeability to Ca^{2+} ions

We examined the response of cholangiocytes to hypotonic stress (160 $mOsm.L^{-1}$) using Fura-2-AM ratio live imaging and measure of Ca^{2+} signals **(Fig. 1A)**. Cholangiocytes maintained a stable $[Ca^{2+}]_i$ when in isotonic buffer but showed a slow rise in intracellular Ca^{2+} when bathed with the hypotonic solution (**Fig. 1B**). The onset of hypotonic responses followed a variable lag period such that individual cell responses often occurred asynchronously. On average, 74±6% (range from 63 to 92%) of cholangiocytes were responsive to hypotonic stress (**Fig. 1B,E**). Both responsive and non-responsive cholangiocytes to hypotonic shock showed similar responses to ATP application (150µM), indicating that non-responsive cells were healthy (**Fig. 1C**). In contrast, cholangiocytes showed no propensity to respond to hypertonic stress (**Supplemental Fig. 1D,E**).

Hypotonic solution-induced Ca^{2+} responses were markedly reduced in Ca^{2+}-free solution (**Fig. 1D**). Only 27% of cholangiocytes still responded to hypotonic solution under this condition (**Fig. 1E**), with a mean peak Δratio reduced by 30% (**Fig. 1F**). In addition, most cholangiocytes gave a single Ca^{2+} spike in response to hypotonic stress in Ca^{2+}-free conditions (**Fig. 1D**). As a result, there was a 60% reduction in the area under the curve (AUC) of the hypotonic stress-induced Ca^{2+} responses (**Fig. 1G**). Interestingly, purinergic responses also displayed spike-like waveforms in Ca^{2+}-free solution, reminiscent to hypotonic Ca^{2+} responses recorded likewise (**Fig. 1D, H-I**). Collectively, these data indicate that hypotonic stress induces slow Ca^{2+} signals in cholangiocytes, which mainly depend on external calcium influx.

Primary cilium has no role in sensing hypotonic stress

At DIV5, 28% of CK19-positive cells exhibited a primary cilium, as evidenced by acetylated tubulin staining (**Supplemental Fig. 2A,B**). Because primary cilia may sense modifications in osmolarity (Masyuk et al., 2008; Larusso and Masyuk, 2011), we tested whether deletion of the primary cilium could alter hypotonic responses. Incubation of cells with 4mM chloral hydrate for 24h resulted in the almost complete loss of primary cilia in CK19-expressing cells **(Supplemental Fig.2C,E)**. This treatment had no deleterious effects on the proportion of CK19-expressing cells (**Supplemental Fig.2D**). Chloral hydrate incubation had no effect on the proportion of cholangiocytes responding to hypotonic shock, nor on the amplitude of Ca^{2+} responses (**Supplemental Fig.2F-H**). However, we observed a significant reduction of the amplitude of purinergic Ca^{2+} signals (**Supplemental Fig.2I**), perhaps indicative of the presence of a subset of purinergic receptors located on the cholangiocyte cilium (Larusso and Masyuk, 2011). Collectively, these data indicate that the primary cilium is not required for signaling hypotonic stress.

Hypotonic stress-induced Ca^{2+} signals depend on ATP release acting primarily on P2X4 receptors

To probe the molecular mechanism that mediates plasmalemmal Ca^{2+} influx under hypotonic conditions, we tested the effects of apyrase, an ATP-diphosphohydrolase that catalyzes the hydrolysis of ATP. Apyrase (5U/mL) added to hypotonic buffer reduced the proportion of hypotonic solution responding cells from 73.5 to 56.5% (**Fig. 2A,B**) and the mean amplitude/AUC of the responses by ~30% (**Fig. 2C,D**). We confirmed that apyrase,

at the concentration used, abolished the response to exogenous ATP (150 µM, **Fig. 2E,F**).

We found that mouse cholangiocytes at DIV5 express transcripts for P2X1, P2X2, P2X4, P2X5 and P2X7 receptor subtypes (**Fig. 2G**). However the non-selective P2R antagonist suramin at 20 µM, a concentration that should affect most subtypes, excepted P2X7R and P2X4R subtypes (IC_{50} is >100 µM; North and Jarvis, 2013), had no significant inhibitory effects on hypotonic Ca^{2+} responses, (**Supplemental Fig. 2J,K**). Suramin was efficient at relatively high concentrations (200 µM), suggesting the involvement of P2X7R and P2X4R subtypes (**Supplemental Fig. 2J,K)**. Therefore, we studied in detail the effects of the selective P2X7R antagonists A804598 and A740003, which have IC_{50} values of 10 and 50 nM for rodent P2X7R, respectively (Donnelly-Roberts et al., 2009). Both A-compounds, used at 10-fold the IC_{50}, had no inhibitory effects on hypotonic Ca^{2+} responses (**Fig. 2H-K**). Interestingly, they also had modest effects on ATP-induced Ca^{2+} responses, providing further support that P2X7R does not contribute a major component of purinergic signaling (**Fig. 2L**).

We further tested the effects of the P2X4R antagonist 5-BDBD that exhibits no significant antagonist effects at other P2XRs (Coddou et al., 2019). 5-BDBD reduced by ~50% both the amplitude and AUC of hypotonic responses (**Fig. 2M-P**). Interestingly, 5-BDBD also inhibited Ca^{2+} responses evoked by exogenous ATP by the same amount (**Fig. 2Q**). Altogether, these findings suggest that the P2X4R contributes to the ATP-dependent hypotonic calcium response.

The mechanosensitive ion channel Piezo1 is functionally active in mouse cholangiocytes

As a first step towards identifying the plasmalemmal channel(s) that senses hypoosmotic challenge and primes ATP release, we applied Gd^{3+} (50 μM), a broad-spectrum inhibitor of stretch-activated ion channels. Under Gd^{3+} application, 85% of cholangiocytes were unresponsive to hypotonic shock (**Fig. 3A,B**). The few remaining responsive cells had reduced peak responses with features reminiscent to those seen in Ca^{2+} free solution (**Fig. 3A,C-D**, compare with **Fig. 1D**).

Multiple putative mechanosensitive ion channels are known to be expressed in cholangiocytes, however with the notable exception of TRPV4 there is little evidence supporting any of these as a component of the osmosensitive transduction complex. With the use of RT-PCR assay from DIV5 primary cultures, we detected RNA for the vanilloid subtypes TRPV2 and TRPV4, the members of the polycystin-like groups TRPP1 and TRPP2 (Delmas, 2004) and the mechanosensitive ion channel Piezo1 (Coste et al., 2010) (**Fig. 3F** and **Supplemental Fig.3A**). mPiezo1 was detected with different sets of primers (see Methods), whereas Piezo2 was barely detectable (**Supplemental Fig.3A**). Immunostaining using a polyclonal Piezo1 antibody (Thermo Fisher Scientific, Methods) further showed labeling of cholangiocytes (**Fig. 3E**). To verify that the antibody interacts with the intended target we transfected *mpiezo-GFP* in Piezo1-deficient (P1KO) HEK293T cells. Strong immunoreactivity for Piezo1 was found in HEK293T-P1KO cells that have been effectively transfected (**Fig. 3E**). Unfortunately, no specific banding was observed in western blots from Piezo1-transfected HEK293T-P1KO cells with this anti-Piezo1 antibody. The same hold for the 5 other commercially available antibodies tested (see Methods). However, using immunoprecipitation with the ThermoFisher anti-Piezo1

antibody coupled to mass spectrometry, we identified mPiezo1 peptide sequences from lysates of DIV5 cholangiocytes (**Supplemental Fig.3B**).

To stimulate Piezo1 channels, we used the Piezo1 agonist, chemical compound Yoda1, which is selective for Piezo1 over Piezo2 (Botello-Smith et al., 2019; Syeda et al., 2015). Bath application of Yoda1 in DIV5 cholangiocytes evoked robust Ca^{2+} signals (**Fig. 3G**). Approximate EC_{50} for Yoda1 in cholangiocytes was 29.4 ± 1.25 μM (**Fig. 3H**), which compares well with EC_{50} of 17.1 and 26.6 μM for murine and human piezo1-transfected HEK293T cells, respectively (Syeda et al., 2015). Yoda1 signal was dependent on extracellular Ca^{2+} in cholangiocytes (**Fig. 3I**) and exclusively related to the expression of Piezo1 since Yoda1 had no effects on HEK293T-P1KO cells (**Fig. 3J,K**).

Piezo1 contributes to hypotonic stress-induced Ca^{2+} signals in cholangiocytes

To test whether Piezo1 contributes to hypotonicity-induced Ca^{2+} responses, we inhibited endogenous Piezo1 by using specific *piezo1*-siRNAs targeting four distinct sequences of *piezo1* mRNA. Quantification of mRNA transcripts and data normalization were carried by qPCR against the invariant endogenous housekeeping genes GAPDH, β-Actin and CK19. As shown in **Figure 4A**, *piezo1* mRNA level decreased two-fold in *piezo1*-siRNA-transfected cholangiocytes compared with those transfected with scrambled siRNAs. Accordingly, *Piezo1*-siRNA significantly reduced the responses of cholangiocytes to Yoda1 exposure (**Fig. 4B-D**). *Piezo1*-siRNA also reduced the proportion of cholangiocytes responding to hypotonic stress and the peak/AUC of the responses (**Fig. 4E-H**). Collectively, these data suggest that Piezo1 activation contributes to hypotonic calcium responses. Consistent with a role in osmosensation, overexpression of mPiezo1

promoted hypotonic responses in characteristically unresponsive HEK293T-P1KO cells to hypotonic stimulation (**Fig. 4I-K**).

Hypotonic stress-induced activation of Piezo1 promotes ATP release

Whether ATP release induced by hypotonic stimulation was subsequent to Piezo1 activation was first assessed by pharmacological assays. Using the luciferase-ATP bioluminescent detection assay, we detected a 6-fold increase in ATP release, from 2.85±0.43 to 17.58±2.28 nM (n=10) following hypotonic stimulation (**Fig. 5A**). ATP release was inhibited by about 30% by Gd^{3+} (100µM) and GsMTx4 (5µM), a peptide from tarantula venom effective against Piezo1 at low micromolar concentrations (Suchyna et al., 2000) (**Fig. 5A**). Because none of these inhibitors are piezo-specific, we tested whether *piezo1*-siRNAs could inhibit hypotonic stress-induced ATP release. ATP secretion was decreased by 46% in *piezo1*-siRNA-treated cholangiocytes compared with control-siRNA treated cells (**Fig. 5B**).

To further investigate Piezo1-dependent ATP release, we examined Ca^{2+} mobilization upon exposure to Yoda1. One trait of Yoda1 responses was their biphasic shape composed of an initial rise in $[Ca^{2+}]_i$, concurrent with Yoda1 application, followed by a delayed, slow $[Ca^{2+}]_i$ increase (**Fig. 5C**). The delayed 'rebound' response often outperformed the initial Yoda1 response. Importantly, when apyrase was applied concurrently with Yoda1, only the initial phase was significantly diminished (**Fig. 5D-F**). However, the delayed response was impaired when apyrase was maintained beyond Yoda1 exposure, but resumed as soon as apyrase was washed out (**Fig. 5G**). Consequently, there was a clear relationship between the occurrence of the delayed

phase and the duration of apyrase application (**Fig. 5H**). Another manifestation of sustained ATP release induced by Yoda1 was the observation that cholangiocytes became refractory to ATP stimulation following exposure to Yoda1 (**Fig. 5I**). Consequently, amplitude of ATP responses was inversely correlated with the concentration of Yoda1 (**Fig. 5J**). Collectively, these data indicate that Piezo1 activation by Yoda1 promotes long-lasting ATP release.

Piezo1 is not the ATP secretion pathway

Does Piezo1 by itself qualify as a permeation pathway for ATP? To answer this question we took advantage of the fact that Yoda1 did not generate Ca^{2+} responses in HEK293T-P1KO cells. However, Yoda1 caused large Ca^{2+} signals in HEK293T-P1KO cells overexpressing mPiezo1 (see **Fig. 3J**). Importantly in these cells, Yoda1-induced Ca^{2+} signals were not inhibited by apyrase (**Supplemental Fig.4A,B**), suggesting that ATP does not amplify Yoda1-induced Ca^{2+} responses in mPiezo1-expressing HEK293T-P1KO cells, although they express P2X4R (**Supplemental Fig.4C**). As a corollary, no secretion of ATP was detected in response to Yoda1 application in HEK293T cells, HEK293T-P1KO cells, and HEK293T-P1KO cells overexpressing mPiezo1 (**Supplemental Fig.4D,E**). These observations are all suggestive of a channel-mediated ATP release mechanism distinct from Piezo1.

Piezo1-driven activation of Pannexin1 mediates ATP release

We found strong expression of Panx1 in DIV5 cholangiocytes using RT-PCR, immunocytochemistry and western blots (**Supplemental Fig.5A-C**). We investigate the role of Panx1 using carbenoxolone (CBX) and probenecid (PBC), which are well known to inhibit Panx1-mediated ATP release in a variety of systems (Locovei et al., 2006; Silverman et al., 2008). Pretreatment of cholangiocytes with CBX or PBC decreased the secretion of ATP induced by hypotonic stimulation by about 50% (**Fig. 6A**). PBC also decreased the proportion of cholangiocytes that responded to hypotonic stress along with the amplitude of the Ca^{2+} responses (**Fig. 6B-E**). Likewise, CBX also decreased significantly the proportion of cholangiocytes responsive to hypotonic stimulation from 89% in control to 51% with CBX (**Fig. 6F)**. In addition, PBC reduced Yoda1-induced Ca^{2+} responses, acting on both the initial and delayed components of Yoda1 responses (**Fig. 6G-I**). Because PBC may have off-targets, we confirmed that PBC had no direct effects on Piezo1 since Yoda1-induced responses in HEK293T-P1KO cells overexpressing Piezo1 were not impaired (**Fig. 6J,K**). Collectively, these findings identify a role for Panx1 in ATP secretion secondary to hypotonic stimulation of Piezo1.

Piezo1 and Panx1 can assemble within a protein complex

We investigated potential interactions between Piezo1 and Panx1 by co-immunoprecipitation in HEK293T-P1KO cells expressing GFP-tagged mPiezo1 and Flag-tagged mPanx1. Expression of epitope tagged proteins was confirmed by Western blotting using antibodies raised against the appropriate epitope tag. Piezo1 was detected as a monomeric ≈290kDa immunoreactive band whereas Panx1 was detected as a double

band of 42-44 and 44-47 kDa (**Fig. 7A, Supplemental Fig.5C**). A similar band pattern has been observed on Western blotting for Panx1 in 9 independent experiments, and may reflect differential S-nitrosylation and glycosylation states (Lohman et al., 2012). When an anti-flag antibody was used to immunoprecipitate flag-tagged Panx1, GFP-tagged mPiezo1 was found to be co-immunoprecipitated (**Fig. 7A**). If Piezo1 is truly able to co-associate with Panx1, then it should also be possible to demonstrate the presence of Panx1 in samples immunoprecipitated using an anti-GFP antibody. To directly test this prediction, we carried out a reciprocal immunoprecipitation protocol, using the same transfected HEK293T-P1KO cell lysates described above. When the anti-GFP antibody was used to immunoprecipitate GFP-Piezo1, flag-tagged mPanx1 was co-immunoprecipitated, consistent with an interaction (**Fig. 7B**). Neither Piezo1, nor Panx1 immunoreactivity was detected in control experiments with a rabbit polyclonal antibody recognizing an unrelated epitope (anti-Ki67 antibody) (**Fig. 7C, left panel**). As additional controls, Panx1 immunoreactivity was not detected in anti-GFP immunoprecipitates from lysates of cells co-transfected with GFP and flag-tagged mPanx1 cDNAs (**Fig. 7C, right panel**).

We further attempted to isolate Piezo1 immunocomplexes from native cholangiocytes, but this turned to be a challenge due to the low level of Piezo1 protein under natural expression levels. Therefore, we took advantage of the use of an immortalized cell line of murine cholangiocytes that retains characteristics similar to those of freshly isolated cholangiocytes (Ueno et al., 2003). When the ThermoFisher anti-Piezo1 antibody was used to immunoprecipitate Piezo1, Panx1 was found to be present in Piezo1 immunocomplexes (**Fig. 7D**).

Our findings therefore suggest that Piezo1 and Panx1 can be isolated in a stable complex by co-immunoprecipitation. To assess whether these complexes may localize in plasma membrane domains, we dually transfected Piezo1-GFP and Panx1-flag in HEK293T-P1KO cells. Subsequent analysis of the immunostained tags using confocal microscopy showed patterns of membrane co-localization (**Supplemental Fig. 5D**). Profile analysis across co-transfected cells showed dense fluorescence intensity at the cell periphery (**Supplemental Fig.5E**). We confirmed the absence of detectable immunostaining in cells not expressing the cognate protein, demonstrating the specificity of both the primary and secondary antibodies (data not shown). The observed overlapping distribution is consistent with our prediction that these two proteins may interact in plasma membrane domains.

Co-expression of mPiezo1, Panx1 and P2X4R reconstitutes a functional ATP-secreting protein complex

We co-transfected mPiezo1-GFP, mPanx1-HA and P2X4R-myc in HEK293T-P1KO cells to reconstitute functional complexes. Subsequent analysis of immunostained tags using confocal microscopy showed successful co-expression of the 3 proteins at the cell periphery (**Supplemental Fig. 6A**). Yoda1-induced Ca^{2+} responses in these cells were markedly augmented compared with HEK293T-P1KO cells expressing only mPiezo1-GFP or mPiezo1-GFP and mPanx1-HA (**Supplemental Fig. 6B),** suggesting stimulation of P2X4Rs by released ATP. Consistently, application of exogenous ATP caused a massive calcium signal (+218% on average), confirming the effective expression of P2X4Rs. On average, Yoda1 responses in cells expressing the 3 proteins were significantly increased by 119 and 45% compared to responses in cells expressing mPiezo1-GFP alone or mPiezo1-GFP and mPanx1-HA (**Supplemental Fig. 6C).** Moreover, apyrase reduced Yoda1 signals in cells co-expressing the 3 proteins, and produced overshooting Ca^{2+}

responses on washout, indicative of ATP release and stimulation of P2X4Rs (**Supplemental Fig. 6D)**.

Discussion

Utilizing molecular, pharmacological, and functional approaches the present study identifies a new pathway for osmosensation and ATP secretion in cholangiocytes. We show that Piezo1 serves as an osmosensor triggering $[Ca^{2+}]_i$ increase and subsequent activation of Panx1, which acts as ATP-conducting pathway. This chain of events leads to signal amplification through stimulation of autocrine/paracrine P2X4R. Collectively, these data provide a new working model for mechanosensitive secretion of ATP in bile ducts (**Fig. 8**).

Hypotonic Ca^{2+} responses occur through cilium-independent pathways and P2X4R stimulation

Our data indicate that mouse cholangiocytes are sensitive to hypotonic but not hypertonic challenges. Hypotonic responses are based on membrane deformation following the swelling of the cell by water influx (Wang et al., 1996). At variance with previous work (Gradilone et al., 2007), we found that hypotonic Ca^{2+} responses do not require the primary cilium. This discrepancy may be related to the difference in methodological approaches or preparations. Nevertheless, there are many precedents for cilium-independent osmotic responses and ATP release in many cell types (Rodat-Despoix et al., 2013; Iomini et al., 2004), including cholangiocyte-derived cells (Woo et

al., 2008). While our data suggest that hypotonic response occurs through a cilium-independent pathway, they do not discount a contribution of the primary cilium in the response to shear stress (Gradilone et al., 2007).

We found that hypotonic Ca^{2+} responses were essentially dependent on extracellular calcium. In few instance, residual Ca^{2+} responses were observed in free $[Ca^{2+}]_o$, suggesting that P2YRs, linked to inositol triphosphate-mediated release of Ca^{2+} from intracellular endoplasmic reticulum stores, may contribute a minor component of the hypotonic Ca^{2+} response (Hirata et al., 2002; Dutta et al., 2008). Yet, we found that propagation of Ca^{2+} waves from stimulated cholangiocytes to the neighboring cells prominently relies on the autocrine/paracrine action of ATP on P2X4R, the dominant subtype in rodent cholangiocytes (Doctor et al., 2005; Woo et al., 2010). P2R stimulation is known to increase transepithelial Cl^- secretion and to contribute to transport of water and HCO_3^- in both rodent and human biliary epithelial models (Roman et al., 1999; Zsembery et al., 1998). Thus, stimulation of P2X4R may be an important regulatory step linking membrane-directed forces to coordinated cholangiocyte responses regulating bile formation and secretion.

Piezo1 serves as an osmosensor in cholangiocytes

Piezo1 has been involved in mechanosensitive ATP release pathways in different cell systems (Cinar et al., 2015; Miyamoto et al., 2014; Wang et al., 2016; Diem et al., 2020). Here we showed that Piezo1 is an important determinant of mechanosensation in mouse cholangiocytes. Piezo1 is endowed with properties that make it a likely candidate for a cholangiocyte osmosensor (Coste et al., 2010; Ranade et al., 2015).

Downregulation of Piezo1 by siRNAs resulted in substantial inhibition of both hypotonic Ca^{2+} responses and ATP secretion. We obtained similar inhibitory effects with the spider toxin blocker, GsMTx4, and gadolinium, although both might have off targets. Additionally, activation of Piezo1 by Yoda1 induced long-lasting Ca^{2+} responses in cholangiocytes, which require ATP secretion and P2XR signaling. Collectively, these data indicate that Piezo1 contributes to hypotonic Ca^{2+} responses and ATP release in cholangiocytes.

Previous search for osmosensitive ion channels in cholangiocytes pointed to the involvement of TRPV4 located on the primary cilium (Gradilone et al., 2007). More recently, TRPV4 has also been shown to translate fluid flow into intracellular signaling and biliary secretion (Li et al., 2020). It is therefore plausible that both Piezo1 and TRPV4 serve as mechanosensors in cholangiocytes as neither Piezo1 (this study) nor TRPV4 (Gradilone et al., 2007) knock-down abolished hypotonic Ca^{2+} responses. Thus, the presence of different mechanosensors endows cholangiocytes with the aptitude to distinguish different mechanical stimuli, and eventually to signal them differentially.

Piezo1 – Panx1 complex couples force detection to ATP secretion

Our data indicate that Piezo1 is necessary but not sufficient for ATP secretion. Previous studies have proposed two nonexclusive mechanisms for ATP secretion in cholangiocytes, that is, exocytosis of ATP enriched vesicles and release through ATP-permeable CFTR channels (Fitz, 2007). Our investigation is suggestive of an additional

mechanism involving Panx1-mediated ATP release. Supporting this idea, we found that pharmacological inhibition of Panx1 strongly reduced ATP secretion in response to both hypotonic stress and Yoda1 exposure. A broad set of experimental evidence indicates that Panx1 can mediate ATP release under physiological and pathological conditions in a variety of cell types (Dahl, 2015). Panx1 can form a transmembrane channel called pannexon, permitting ATP efflux from cells down its concentration gradient.

How might Piezo1 regulate the function of Panx1 channels? Prior studies have shown that increase in cytoplasmic Ca^{2+} concentration can activate Panx1 (Locovei et al., 2006). A tantalizing hypothesis is therefore that calcium influx mediated by Piezo1 provides a triggering mechanism for Panx1 activation. This functional relationship may be enhanced by physical promiscuity. By a combination of immunocytochemistry and co-IP techniques, we were able to provide evidence that both proteins can colocalize and interact physically in recombinant systems and normal mouse cholangiocytes. Although these findings suggest an ability to interact - directly or through intervening proteins – we could not demonstrate whether the Piezo1-Panx1 complex exists in native cholangiocytes. Thus, whether Piezo1 physically interacts with Panx1 in native cholangiocytes will have to be resolved in further studies.

In conclusion, the present study was initiated to explore stretch sensitive mechanisms and ATP release in cholangiocytes. Our data are consistent with the idea that both Piezo1 and Panx1 molecules are necessary for eliciting downstream effects of hypotonic stress. By mediating a rise in intracellular Ca^{2+}, Piezo1 acts as a mechanosensor responsible for translating cell swelling into activation of Panx1,

activation of which is critical for ATP release. These findings provide new insight into the molecular mechanisms controlling ATP secretion and may facilitate the development of novel therapeutic strategies for liver diseases.

Materials and Methods

Animals. All animals were used in accordance with the European Community guiding in the care and use of animals (2010/63/UE). Experiments were performed in accordance with the French government regulations.

Osmotic solutions. The Krebs solution consisted of (mM): 130 NaCl, 3 KCl, 1 $MgCl_2$, 10 Hepes, 10 glucose and 2.5 $CaCl_2$ (290±5mOsm.L^{-1}). The isotonic external solution (ISO) consisted of (mM): 65 NaCl, 3 KCl, 1 $MgCl_2$, 2.5 $CaCl_2$, 10 Hepes, 10 glucose, 120 mannitol (290±5 mOsm.L^{-1}). The hypotonic solution (160±55 mOsm.L^{-1}) was generated by removing mannitol to the ISO solution, whereas the hypertonic solution (460.5 mOsm.L^{-1}) was prepared by adding mannitol to the Krebs solution. Ca^{2+}-free solutions were prepared by omitting $CaCl_2$, no EGTA was added.

Primary cultures from mouse IBDUs. Primary cultures of cholangiocytes from IBDUs were obtained mainly as described (Mennone et al., 1995). Male C57Bl6 mice aged 10-20 weeks were used for isolation of the biliary tree. Mice were anesthetized with isoflurane and sacrificed by decapitation. The liver was perfused through the portal vein for 5 min with PBS and then for 20 min with PBS containing 1 mg/mL collagenase D (Sigma #COLLD-RO) and 100 µM CaCl2. After careful removal of the Glisson's

capsule, the intrahepatic biliary tree was isolated by repeated washes in PBS and thinly minced with scissors in PBS supplemented with 2 mg/mL collagenase D, 0.32 mg/mL pronase (Sigma #PRON-RO), 0.04 mg/mL DNase (Sigma #DN25), 1% fetal bovine serum (FBS, Gibco #10270) and 1% penicillin/streptomycin (P/S, Gibco #15140-122). These pieces were digested for 45 min at 37°C and then mechanically dissociated and sifted in a 100 µm cell-strainer. After centrifugation, cells were resuspended in PBS supplemented with 2 mg/mL collagenase D, 0.34 mg/mL Hyaluronidase (Sigma #H3506), 0.04 mg/mL DNase, 1% FBS and 1% P/S. Cells were incubated for 20 min at 37°C. Finally, cells were seed on rat-tail type-I collagen (Corning) coated Petri dishes or coverslips with DMEM/F-12 medium (Gibco #31331-028) supplemented with 3.6% heat-inactivated FBS, 1% P/S and 1‰ gentamicin (Gibco #15750-037) and incubated at 37°C in a CO2-equilibrated incubator. A small subset of cells, negative for CK19 and albumin, was detected in IBDU cultures using phalloidin staining. They had elongated cell body with bundles of F-actin terminating at the cell surface typical of fibroblasts (data not shown). Deciliation of cholangiocytes were achieved by incubation with 4 mM of chloral hydrate for 24h (Masyuk et al. 2006).

Cultures of cell lines and transfection. HEK cells (293T and P1KO) and Normal Mouse Cholangiocytes (NMCs) were cultured in DMEM containing 10% heat-inactivated fetal bovine serum and 1% penicillin/streptomycin. *Piezo1*-deficient (P1KO) HEK293T cells were generated using CRISPR/Cas9 nuclease genome engineering (Lukacs et al., 2015). Plasmid transfection (m*Piezo*1iresGFP; m*Piezo1-GFP*; pCMV3-N-*GFPspark*, m*Panx1-flag*) was achieved using lipofectamine 2000 with 1.2µg/mL of plasmids.

Calcium imaging. Cholangiocytes or HEK cells, grown on collagen type I-coated coverslips, were loaded with Fura-2-AM (2μM) for 45 or 30 min, respectively, at 37°C in Krebs solution (Rodat-Despoix et al., 2013). Fura-2-AM loaded cells were placed on the stage of an inverted epifluorescence microscope (Olympus IX71) equipped with a ×20, UPLSAPO objective and continuously superfused. Fura-2AM was alternately excited at 340 and 380 nm, and ratio of the resulting images (340nm/380nm) were produced every 1 s. The source of excitation light was a xenon arc lamp, and excitation wavelength was selected by a fast excitation filter wheel (Illumination Systems MT20, Olympus). Digital images were sampled at 12-bit resolution by a fast-scan, cooled charge-coupled device (B/W CCD) digital camera (Orca-ER, Hamamatsu). All the images were background subtracted and controlled by Cellˆ R software (Olympus). A positive response was defined as a signal at least twice larger than the Δratio deviation determined from 3 min recording of the standard baseline. The peak ratio value was determined as the difference (Δratio) between the maximum peak value and the baseline, during hypotonic shock or drug application. The area under the curve (AUC) above baseline was determined using a trapezoidal method for the duration of drug application. Dose-response curve for Yoda1 was obtained from different experimental sets of coverslips that were prepared from different animals on different days. Dose-response curves were fitted to the data using nonlinear regression. The recording traces in the figures show representative examples of the effect of the drug/test of interest. The histograms/bar charts show pooled data from individual cells (n), collected from independent experiments (N). The numbers of cells analyzed in each of these independent experiments and the corresponding average responses are presented in the Supplemental Table 4.

Gene silencing by siRNA. Cholangiocytes at DIV1 were transfected for 7h with lipofectamine RNAimax, 10nM of *Piezo1*-siRNA or scrambled siRNA and 2nM of siGLO Red Transfection Indicator without serum and antibiotic. SiRNAs are listed in the Supplemental Information (Table 1).

Immunostaining. Cholangiocytes, HEK.P1KO and HEK293T cells, cultured on (Collagen I and poly-D-lysin, respectively) coated glass coverslips, were first washed with PBS and fixed using 4% paraformaldehyde for 10min, permeabilized in PBS containing 0.1% Triton X-100 for 10min, blocked with 3% (v/v) gelatin for 1h and incubated with primary antibodies at 4°C overnight. After washes, cells were incubated with secondary antibodies (1:1000) at RT for 1h and nucleus were stained using DAPI for 10min. Primary and secondary antibodies are listed in the Reagents and Tools table below.

Reverse Transcriptase-PCR. Total RNA was extracted from DIV5 cholangiocytes and NMC with Trizol Reagent according to the manufacturer's recommendation. ARN concentration was measured using a NanoDrop ND-2000 Spectrophotometer. Four micrograms of total RNA were treated with DNaseI and RT reactions with oligo(dT)$_{20}$ primers were performed with the SuperScriptIII® First-Strand Synthesis System kit. PCR was performed with *Taq* DNA Polymerase. Sequences of PCR primers are listed in the Supplemental Information (Table 2).

Real time RT qPCR. Total RNA extraction and DNase treatment of cholangiocytes were achieved with NucleoSpin®RNA kit according to manufacturer's instructions. RT reactions were performed as described above. qPCR reactions were run in duplicate using Kapa Sybr® Fast qPCR kit on an Applied Biosystems 7500 Fast Real-time PCR thermocycler. Sequences of specific primers are listed in the Supplemental Information, Table 3. The Relative Quantification (RQ) method was used to compare the relative expression of *Piezo1* gene between siCtr- and siPiezo1-transfected cholangiocytes.

Extracellular ATP measurements. Detection of released ATP was performed using luciferin/luciferase detection assay using a spectrofluorimeter-luminometer (Tecan infinite F500). IBDU and HEK cells were cultured in black 96-well Greiner dishes with clear bottoms. ATP secretion was estimated in stimulated and unstimulated cells after a 15min-incubation period with luciferin/luciferase diluted at 1/25 for 5 min. To determine the concentration of ATP, a calibration curve was constructed using known concentrations of ATP (0.02-200 nM).

Immunoprecipitation from transfected HEK.P1KO cells. Protein extraction is detailed in the supplementary Materials and Methods. Protein A magnetic beads were coated with 5µg of rabbit polyclonal anti-GFP antibody or 10µg of rabbit polyclonal anti-flag antibody or 10µg of rabbit polyclonal anti-Ki67 antibody (negative control) by rotating at RT for 10min. Cells were added to the beads and rotated for 1h. Protein complexes were purified by magnetisation of the beads and washed with PBS-Tween 0.1% at RT.

Proteins were eluted from beads by adding Laemmli denaturation sample buffer and incubated 10min at 70°C.

Immunoprecipitation from DIV5 cholangiocytes and NMCs. DIV5 cholangiocytes were harvested using TrypLE express and pelleted by centrifugation at 300g for 4min. Following protein extraction, immunoprecipitation was performed with Dynabeads™ co-immunoprecipitation kit according to manufacturer's instructions. The primary antibodies, rabbit polyclonal anti-Piezo1 (Fisher) and rabbit polyclonal anti-Ki67 (7µg/mg of beads) were covalently linked to magnetic beads. The extraction buffer was supplemented by adding 150mM NaCl, 20mM Nethylmaleimide, 1.2% Triton and a cocktail of protease inhibitors without EDTA. Proteins were eluted from beads by adding Laemmli denaturation Sample Buffer and incubated 10min at 70°C.

Western Blot. Protein samples were denaturated by adding 0.1M DTT, 3M urea and 10min boiling at 99°C. Protein samples were loaded in polyacrylamide gel and transferred on a nitrocellulose membrane (GE Healthcare Life science). Proteins were controlled by Ponceau staining (0.2% w/v Ponceau diluted in 5% glacial acetic acid). Membranes blocked with 5% milk diluted in TBST for 1h at RT and probed with primary antibodies overnight at 4°C. The antibodies used are detailed in the supplementary Materials and Methods. After washing with TBST, the membranes were incubated for 1h with HRP-coupled goat anti-mouse (1:1000) or anti-rabbit secondary antibodies. HRP was revealed by chemiluminescence with blotting substrate POD (1:100) and membranes were scanned on iBright CL750 imaging system.

Mass Spectrometry on DIV5 cholangiocyte immunocomplexes. See Expanded View Materials and Methods

Chemicals. Stocks of chemicals were reconstructed in either DMSO (5-BDBD, 1mM; probenecid, 100mM; A-804598, 10mM; A-740003, 10mM) or in PBS (ATP, 50mM; chloral Hydrate, 1M; gadolinium, 1mM; apyrase, 100U/mL; suramin, 50mM; carbenoxolone, 250mM; GsMTx4, 100µM) and stored at 4 or -20°C. Yoda1 was dissolved in 75% DMSO – 25% PBS (v/v) at 10mM and stored at -20°C.

Statistical analysis. Data were expressed as mean ± S.E.M. Tests for differences between two normally distributed populations were performed using two-tailed Student's *t*-test and differences in percentages were analyzed by Fisher exact test (GraphPad; Prism 7.00). To compare more than two conditions, data were analyzed by ANOVA and Dunnett's post-test. P values ≤ 0.05 were considered significant.

Reagents and Tools Table

Reagent/Resource	Reference or Source	Identifier or Catalog Number
Experimental Models		
C57Bl6 mice	Janvier Labs and inbred colonies	https://www.janvier-labs.com/fiche_produit/souris-c57bl-6jrj/
HEK293t cells	ATCC	Cat# CRL-3216
HEK.Piezo1KO cells	Dr. A. Patapoutian, Scripps Research Institute	Lukacs et al. Nat commun. 2015
NMC cells	Dr. Shannon Glaser, Texas A&M University System Health Science Center	N/A
Recombinant DNA		

mouse Piezo1iresGFP	This paper	N/A
mouse Piezo1-GFP	A. Patapoutian	Coste et al. Nature 2012
pCMV3-N-GFPspark	Interchim	Cat# CV027
mouse Panx1-flag	Interchim	Cat# MG52303-CF
Antibodies *IF: immunofluorescence;* *IP: immunoprecipitation;* *WB: western blot*		
rabbit monoclonal anti-CK-19 IF (1:200)	Abcam	Cat# ab52625
goat polyclonal anti-albumin IF (1:200)	Euromedex	Cat# A90-234A
mouse monoclonal anti-acetylated tubulin IF (1:200)	Sigma Aldrich	Cat# T6793
rabbit polyclonal anti-piezo1 IF (1:100) IP (7 µg/mL of beads) WB (not specific)	ThermoFisher Scientific	Cat# PA5-77617
rabbit polyclonal anti-piezo1 IF (1:50 human isoform) WB (not specific)	Proteintech	Cat# 15939-1-AP
rabbit polyclonal anti-piezo1 IF and WB (not specific)	Alomone	Cat# APC-087
rabbit polyclonal anti-piezo1 IF and WB (not specific)	Origen	Cat# TA309651
rabbit polyclonal anti-piezo1 IF and WB (not specific)	Novus	Cat# NBP1-78537
rabbit polyclonal anti-piezo1 IF and WB (not specific)	Abgent	Cat# AG1563
rabbit polyclonal anti-panx1 IF (1:300) WB (1:400)	Alomone	Cat# ACC-234
rabbit polyclonal anti-Ki67 IP (7 or 10 µg/mL of beads)	Abcam	Cat# ab15580
rabbit polyclonal anti-GFP IF (1:200) IP (5 µg/mL of beads) WB (1:1000)	Abcam	Cat# ab6556
mouse polyclonal anti-GFP IF (1:200)	AbD Serotech	Cat# OCT1820

WB (1:1000)		
rabbit polyclonal anti-flag IF (1:200) IP (10 µg/mL of beads) WB (1:1000)	Abcam	Cat# ab1162
mouse monoclonal anti-flag IF (1:100) WB (1:1000	Sigma Aldrich	Cat# F1804
TRITC-coupled polyclonal donkey anti-rabbit IF (1:1000)	Jackson ImmunoResearch	Cat# 711-025-152
Alexa488-coupled polyclonal donkey anti-goat IF (1:1000)	Invitrogen	Cat# A11055
Alexa488-coupled polyclonal donkey anti-mouse IF (1:1000)	Invitrogen	Cat# A21202
Alexa647-coupled polyclonal donkey anti-mouse IF (1:1000)	Invitrogen	Cat# A-31571
HRP-coupled goat anti-mouse WB (1:1000)	BioRad	Cat# 170-6516
HRP-coupled goat anti-rabbit WB (1:1000)	BioRad	Cat# 170-6515
Oligonucleotides and other sequence-based reagents		
piezo1-siRNA (SMART pool ON-TARGETplus)	Dharmacon	Cat# L-061455-00
scrambled siRNA (ON-TARGETplus Non-targeting pool)	Dharmacon	Cat# D-001810-10
siGLO Red Transfection Indicator	Dharmacon	Cat# D-001630-02
Custom DNA Oligo	Eurofins genomics	This paper
Chemicals, Enzymes and other reagents		
Fura-2-AM	Molecular Probes	Cat# F1221
Lipofectamine 2000	Invitrogen	Cat# 11668
Lipofectamine RNAimax	Invitrogen	Cat# 13778
5-BDBD	Sigma Aldrich	Cat# SML0450
probenecid	Sigma Aldrich	Cat# P8761

A-804598	Sigma Aldrich	Cat# SML0617
A-740003	Sigma Aldrich	Cat# A0862
ATP	Sigma Aldrich	Cat# A9187
chloral hydrate	Sigma Aldrich	Cat# C8383
gadolinium	Sigma Aldrich	Cat# G7532
apyrase	Sigma Aldrich	Cat# A7646
suramin	Sigma Aldrich	Cat# S2671
carbenoxolone	Sigma Aldrich	Cat# C4790
Yoda1	Sigma Aldrich	Cat# SML1558
GsMTx4	Smartox Biotechnology	Cat# 08GSM001
cold fish gelatin	Sigma Aldrich	Cat# G7765
phalloidin-FITC	Sigma Aldrich	Cat# P5282
Trizol Reagent	Life technologies	Cat# 15596026
DNase I	Invitrogen	Cat# 18068
Taq DNA polymerase	Invitrogen	Cat# 10342020
protéin A magnetic beads	BioRad	Cat # 161-0411
N-ethylmaleimide	Sigma Aldrich	Cat# E3876
protesae inhibitors with EDTA	Roche	Cat# 04 693 116 001
protesae inhibitors without EDTA	Roche	Cat# 11836170001
3-8% precasted polyacrylamide gel	ThermoFisher Scientific	Cat# EA03785BOX
4-12% precasted polyacrylamide gel	ThermoFisher Scientific	Cat# WG1401BOX
nitrocellulose membrane	GE Healthcare Life Science	Cat# 10600002
chemiluminescence substrate POD	Roche	Cat# 11500694001
collagenase D	Sigma Aldrich	Cat# COLLD-RO
pronase	Sigma Aldrich	Cat# PRON-RO
DNase	Sigma Aldrich	Cat# DN25
hyaluronidase	Sigma Aldrich	Cat# H3506
poly-D-lysin precoated coverslips	Corning	Cat# 354086
Rat tail collagen type I	Corning	Cat# 354236
gentamicin	Gibco	Cat# 15750-037
Vetflurane® (isoflurane 1000 mg/g)	Virbac	Cat# GTIN 03597132002653
Software		
ImageJ	Schneider et al., 2012	https://imagej.nih.gov/ij/

Xcellence RT	Olympus	https://xcellence-rt.software.informer.com/download/
ZEN	Zeiss	https://www.zeiss.fr/microscopie/produits/microscope-software/zen-lite.html
GraphPad; prism 7.00	GraphPad software Inc.	https://www.graphpad.com/
MASCOT software	Matrix science	https://www.matrixscience.com/
Other		
SuperScriptIII® First-Stand Synthesis System kit	Invitrogen	Cat# 18080-051
NucleoSpin® RNA kit	Macherey-Nagel	Cat# 740955.50
Kapa Sybr® Fast qPCR kit	Kapa Biosystems	Cat# KK4601
luciferin/luciferase detection assay	Sigma Aldrich	Cat# FLAAM
Dynabeads™ co-immunoprecipitation kit	Invitrogen	Cat# 14321D

The supplementary information contains the sequences of RT-PCR, siRNA, and qPCR primers, and basic information about immunostaining, immunoprecipitation, western blot and mass spectrometry protocols.

This study includes no data deposited in external repositories.

Acknowledgments

The authors thank Shannon Glaser for sharing the NMC cell line, Ardem Patapoutian for sharing the mpiezo1 clone, Nancy Osorio for critical discussion and Axel Fernandez and Ophélie Picard for technical assistance. This work was supported by the ERA-Net

ERACoSysMed, DYNAFLOW collaborative project (European Commission /Horizon 2020) and by recurrent operating grants from CNRS and Aix-Marseille University.

Author Contributions

A.D., Conceptualization: Equal; Data curation: Lead; Formal analysis: Lead; Writing – original draft: Supporting; Writing – review & editing: Supporting; E.G., Investigation: Supporting; Data curation: Supporting; Formal analysis: Supporting; V.P., Investigation: Supporting; Data curation: Supporting; Formal analysis: Supporting; T.P., Investigation: Supporting; Writing – review & editing: Supporting; B.C., Investigation: Supporting; Writing – review & editing: Supporting. P.D., Conceptualization: Lead; Data curation: Lead; Formal analysis: Lead; Investigation: Lead; Writing-original draft: Lead; Writing-review & editing: Lead.

Conflict of interest

The authors declare no competing interests.

References

Banales, J.M., Huebert, R.C., Karlsen, T., Strazzabosco, M., LaRusso, N.F., and Gores, G.J. (2019). Cholangiocyte pathobiology. Nat Rev Gastroenterol Hepatol *16*, 269-281.

Botello-Smith, W.M., Jiang, W., Zhang, H., Ozkan, A.D., Lin, Y.C., Pham, C.N., Lacroix, J.J., and Luo, Y. (2019). A mechanism for the activation of the mechanosensitive Piezo1 channel by the small molecule Yoda1. Nat Commun *10*, 4503.

Boyer, J.L. (2013). Bile formation and secretion. Compr Physiol *3*, 1035-1078.

Coddou, C., Sandoval, R., Hevia, M.J., and Stojilkovic, S.S. (2019). Characterization of the antagonist actions of 5-BDBD at the rat P2X4 receptor. Neurosci Lett *690*, 219-224.

Cinar E, Zhou S, DeCourcey J, Wang Y, Waugh RE, Wan J. Piezo1 regulates mechanotransductive release of ATP from human RBCs. (2015). Proc Natl Acad Sci U S A. *112*(38):11783-8.

Coste, B., Mathur, J., Schmidt, M., Earley, T.J., Ranade, S., Petrus, M.J., Dubin, A.E., and Patapoutian, A. (2010). Piezo1 and Piezo2 are essential components of distinct mechanically activated cation channels. Science *330*, 55-60.

Dahl, G. (2015). ATP release through pannexon channels. Philos Trans R Soc Lond B Biol Sci *370*.

Delmas, P. (2004). Polycystins: from mechanosensation to gene regulation. Cell *118*, 145-148.

Diem K, Fauler M, Fois G, Hellmann A, Winokurow N, Schumacher S, Kranz C, Frick M. (2020). Mechanical stretch activates piezo1 in caveolae of alveolar type I cells to trigger ATP release and paracrine stimulation of surfactant secretion from alveolar type II cells. FASEB J, 34(9):12785-12804.

Doctor, R.B., Matzakos, T., McWilliams, R., Johnson, S., Feranchak, A.P., and Fitz, J.G. (2005). Purinergic regulation of cholangiocyte secretion: identification of a novel role for P2X receptors. Am J Physiol Gastrointest Liver Physiol *288*, G779-786.

Donnelly-Roberts, D.L., Namovic, M.T., Surber, B., Vaidyanathan, S.X., Perez-Medrano, A., Wang, Y., Carroll, W.A., and Jarvis, M.F. (2009). [3H]A-804598 ([3H]2-cyano-1-[(1S)-1-phenylethyl]-3-quinolin-5-ylguanidine) is a novel, potent, and selective antagonist radioligand for P2X7 receptors. Neuropharmacology *56*, 223-229.

Dutta, A.K., Woo, K., Doctor, R.B., Fitz, J.G., and Feranchak, A.P. (2008). Extracellular nucleotides stimulate Cl- currents in biliary epithelia through receptor-mediated IP3 and Ca2+ release. Am J Physiol Gastrointest Liver Physiol *295*, G1004-1015.

Feranchak, A.P., and Fitz, J.G. (2002). Adenosine triphosphate release and purinergic regulation of cholangiocyte transport. Semin Liver Dis *22*, 251-262.

Fitz, J.G. (2007). Regulation of cellular ATP release. Trans Am Clin Climatol Assoc *118*, 199-208.

Gradilone, S.A., Masyuk, A.I., Splinter, P.L., Banales, J.M., Huang, B.Q., Tietz, P.S., Masyuk, T.V., and Larusso, N.F. (2007). Cholangiocyte cilia express TRPV4 and detect changes in luminal tonicity inducing bicarbonate secretion. Proc Natl Acad Sci U S A *104*, 19138-19143.

Hirata, K., Dufour, J.F., Shibao, K., Knickelbein, R., O'Neill, A.F., Bode, H.P., Cassio, D., St-Pierre, M.V., Larusso, N.F., Leite, M.F.*, et al.* (2002). Regulation of Ca(2+) signaling in rat bile duct epithelia by inositol 1,4,5-trisphosphate receptor isoforms. Hepatology *36*, 284-296.

Iomini, C., Tejada, K., Mo, W., Vaananen, H., and Piperno, G. (2004). Primary cilia of human endothelial cells disassemble under laminar shear stress. J Cell Biol *164*, 811-817.

Larusso, N.F., and Masyuk, T.V. (2011). The role of cilia in the regulation of bile flow. Dig Dis *29*, 6-12.

Li, Q., Kresge, C., Boggs, K., Scott, J., and Feranchak, A. (2020). Mechanosensor transient receptor potential vanilloid member 4 (TRPV4) regulates mouse cholangiocyte secretion and bile formation. Am J Physiol Gastrointest Liver Physiol *318*, G277-G287.

Liedtke, W. (2005). TRPV4 as osmosensor: a transgenic approach. Pflugers Arch *451*, 176-180.

Locovei, S., Bao, L., and Dahl, G. (2006). Pannexin 1 in erythrocytes: function without a gap. Proc Natl Acad Sci U S A *103*, 7655-7659.

Lohman, A.W., Weaver, J.L., Billaud, M., Sandilos, J.K., Griffiths, R., Straub, A.C., Penuela, S., Leitinger, N., Laird, D.W., Bayliss, D.A.*, et al.* (2012). S-nitrosylation inhibits pannexin 1 channel function. J Biol Chem *287*, 39602-39612.

Lukacs, V., Mathur, J., Mao, R., Bayrak-Toydemir, P., Procter, M., Cahalan, S.M., Kim, H.J., Bandell, M., Longo, N., Day, R.W.*, et al.* (2015). Impaired PIEZO1 function in patients with a novel autosomal recessive congenital lymphatic dysplasia. Nat Commun *6*, 8329.

Mansini, A.P., Peixoto, E., Thelen, K.M., Gaspari, C., Jin, S., and Gradilone, S.A. (2018). The cholangiocyte primary cilium in health and disease. Biochim Biophys Acta Mol Basis Dis *1864*, 1245-1253.

Maroni, L., Haibo, B., Ray, D., Zhou, T., Wan, Y., Meng, F., Marzioni, M., and Alpini, G. (2015). Functional and structural features of cholangiocytes in health and disease. Cell Mol Gastroenterol Hepatol *1*, 368-380.

Masyuk, A.I., Masyuk, T.V., and LaRusso, N.F. (2008). Cholangiocyte primary cilia in liver health and disease. Dev Dyn *237*, 2007-2012.

Masyuk, A.I., Masyuk, T.V., Splinter, P.L., Huang, B.Q., Stroope, A.J., and LaRusso, N.F. (2006). Cholangiocyte cilia detect changes in luminal fluid flow and transmit them into intracellular Ca2+ and cAMP signaling. Gastroenterology *131*, 911-920.

Mennone, A., Alvaro, D., Cho, W., and Boyer, J.L. (1995). Isolation of small polarized bile duct units. Proc Natl Acad Sci U S A *92*, 6527-6531.

Miyamoto T, Mochizuki T, Nakagomi H, Kira S, Watanabe M, Takayama Y, Suzuki Y, Koizumi S, Takeda M, Tominaga M. (2014). Functional role for Piezo1 in stretch-evoked Ca^{2+} influx and ATP release in urothelial cell cultures. J Biol Chem., *289*(23):16565-75.

Nauli, S.M., Alenghat, F.J., Luo, Y., Williams, E., Vassilev, P., Li, X., Elia, A.E., Lu, W., Brown, E.M., Quinn, S.J.*, et al.* (2003). Polycystins 1 and 2 mediate mechanosensation in the primary cilium of kidney cells. Nat Genet *33*, 129-137.

North, R.A., and Jarvis, M.F. (2013). P2X receptors as drug targets. Mol Pharmacol *83*, 759-769.

Parpaite, T., and Coste, B. (2017). Piezo channels. Curr Biol *27*, R250-R252.

Pinzani, M., and Luong, T.V. (2018). Pathogenesis of biliary fibrosis. Biochim Biophys Acta Mol Basis Dis *1864*, 1279-1283.

Ranade, S.S., Syeda, R., and Patapoutian, A. (2015). Mechanically Activated Ion Channels. Neuron *87*, 1162-1179.

Rodat-Despoix, L., Hao, J., Dandonneau, M., and Delmas, P. (2013). Shear stress-induced Ca(2)(+) mobilization in MDCK cells is ATP dependent, no matter the primary cilium. Cell Calcium *53*, 327-337.

Roman, R.M., Feranchak, A.P., Salter, K.D., Wang, Y., and Fitz, J.G. (1999). Endogenous ATP release regulates Cl- secretion in cultured human and rat biliary epithelial cells. Am J Physiol *276*, G1391-1400.

Silverman, W., Locovei, S., and Dahl, G. (2008). Probenecid, a gout remedy, inhibits pannexin 1 channels. Am J Physiol Cell Physiol *295*, C761-767.

Suchyna, T.M., Johnson, J.H., Hamer, K., Leykam, J.F., Gage, D.A., Clemo, H.F., Baumgarten, C.M., and Sachs, F. (2000). Identification of a peptide toxin from Grammostola spatulata spider venom that blocks cation-selective stretch-activated channels. J Gen Physiol *115*, 583-598.

Syeda, R., Xu, J., Dubin, A.E., Coste, B., Mathur, J., Huynh, T., Matzen, J., Lao, J., Tully, D.C., Engels, I.H.*, et al.* (2015). Chemical activation of the mechanotransduction channel Piezo1. Elife *4*.

Tabibian, J.H., Masyuk, A.I., Masyuk, T.V., O'Hara, S.P., and LaRusso, N.F. (2013). Physiology of cholangiocytes. Compr Physiol *3*, 541-565.

Taruno, A. (2018). ATP Release Channels. Int J Mol Sci *19*.

Ueno, Y., Alpini, G., Yahagi, K., Kanno, N., Moritoki, Y., Fukushima, K., Glaser, S., LeSage, G., and Shimosegawa, T. (2003). Evaluation of differential gene expression by microarray analysis in small and large cholangiocytes isolated from normal mice. Liver Int *23*, 449-459.

Wang S, Chennupati R, Kaur H, Iring A, Wettschureck N, Offermanns S. (2016). Endothelial cation channel PIEZO1 controls blood pressure by mediating flow-induced ATP release. J Clin Invest.,126(12):4527-4536.

Wang, Y., Roman, R., Lidofsky, S.D., and Fitz, J.G. (1996). Autocrine signaling through ATP release represents a novel mechanism for cell volume regulation. Proc Natl Acad Sci U S A *93*, 12020-12025.

Woo, K., Dutta, A.K., Patel, V., Kresge, C., and Feranchak, A.P. (2008). Fluid flow induces mechanosensitive ATP release, calcium signalling and Cl- transport in biliary epithelial cells through a PKCzeta-dependent pathway. J Physiol *586*, 2779-2798.

Woo, K., Sathe, M., Kresge, C., Esser, V., Ueno, Y., Venter, J., Glaser, S.S., Alpini, G., and Feranchak, A.P. (2010). Adenosine triphosphate release and purinergic (P2) receptor-mediated secretion in small and large mouse cholangiocytes. Hepatology *52*, 1819-1828.

Zsembery, A., Spirli, C., Granato, A., LaRusso, N.F., Okolicsanyi, L., Crepaldi, G., and Strazzabosco, M. (1998). Purinergic regulation of acid/base transport in human and rat biliary epithelial cell lines. Hepatology *28*, 914-920.

Figure legends

Figure 1. Hypotonic stress-induced Ca^{2+} signals in mouse cholangiocytes depend on a plasmalemmal calcium-permeable pathway

A, Left panels: Composition of the Krebs, isotonic and hypotonic solutions. Hypotonic stress is induced by varying the concentration of mannitol, keeping constant the concentration of external ions. Right panels: Recording of Ca^{2+} signals and determination of the response parameters. Responses to individual stimulus were considered positive (i.e. responsive cells) if deflections exceeded twice the standard deviation (dashed blue line) of the baseline (blue line). AUC: area under the curve for the time of stimulus application.

B-C, Changes in fluorescent signals of the ratiometric calcium indicator Fura-2AM in DIV5 cholangiocytes exposed to hypotonic solution. Representative examples of responsive and non-responsive cholangiocytes to hypotonic solution are illustrated in

(**B**) and (**C**), respectively. ATP (150 µM) was applied at the end of the ratio-imaging experiment to monitor cell viability.

D, Hypotonic Ca^{2+} signals in cholangiocytes bathed with a Ca^{2+}-free external solution.

E, Proportion of cholangiocytes showing hypotonic Ca^{2+} responses in the presence or absence of extracellular Ca^{2+}. The number of cells analysed in each condition is indicated. ****, p< 0.0001, Fisher test.

F, **G**, Peak ∆Ratio (340/380nm) **(F)** and area under the curve (AUC) **(G)** of hypotonic Ca^{2+} responses recorded with and without external Ca^{2+}. ***, p= 0.0006; ****, p< 0.0001, unpaired *t*-test.

H, **I**, Peak ∆Ratio (340/380nm) **(H)** and AUC **(I)** of ATP (150 µM)-induced Ca^{2+} responses with and without external Ca^{2+}. ****, p< 0.0001, unpaired *t*-test.

Figure 2. Hypotonic stress induces ATP secretion and subsequent stimulation of P2X4Rs

A, Representative changes of ratiometric Ca^{2+} signals in response to hypotonic stress in two DIV5 cholangiocytes treated (red trace) or not (black trace) with apyrase (5 U/mL).

B, Percentage of cholangiocytes exhibiting hypotonic Ca^{2+} responses in the presence or absence of apyrase. ****, p< 0.0001 (Fisher test).

C, D, Amplitude (**C**) and AUC (**D**) of hypotonic Ca^{2+} responses with and without apyrase. ****, p< 0.0001 (unpaired *t*-test).

E, Paired-pulse ATP stimulation with (red trace) and without (black trace) apyrase. Responses were evoked by two sequential applications of ATP (150μM) elapsed by 20min interval.

F, Paired pulse depression (P2/P1) of ATP responses examined in the presence or absence of apyrase. ****, p< 0.0001, paired *t*-test.

G, Cholangiocytes at DIV5 express a variety of P2XR subtypes, including P2X1, P2X2, P2X4, P2X5 and P2X7 receptors at mRNA level. Black dots indicate 500 bp DNA marker.

H, Hypotonic Ca^{2+} responses of DIV5 cholangiocytes treated with A-804598 (0.1μM, red trace) and A-740003 (0.5μM, blue trace) or its vehicle (DMSO, 0.1%, black trace).

I, Percentage of cholangiocytes showing hypotonic Ca^{2+} responses in the presence of A-804598 (0.1μM), A-740003 (0.5μM) or the vehicle (control). ns, not significant (Fisher test).

J-K, Peak ∆Ratio (**J**) and AUC (**K**) of hypotonic Ca^{2+} responses recorded with prior incubation with A-804598 (0.1μM) or A-740003 (0.5μM). **, p= 0.0027, unpaired *t*-test.

L, Peak ∆Ratio of ATP responses recorded with prior incubation with A-804598 (0.1μM) or A-740003 (0.5μM). ****, p< 0.0001, unpaired *t*-test.

M, Hypotonic Ca^{2+} responses of DIV5 cholangiocytes treated with 5-BDBD (10μM, red trace) or its vehicle (DMSO 0.1%, black trace). Note the reduced amplitude of both hypotonic and purinergic Ca^{2+} responses.

N, Percentage of cholangiocytes showing hypotonic Ca^{2+} responses in the presence of 5-BDBD (10μM) or its vehicle. ns, not significant (p=0.5389).

O,P, Peak ∆Ratio **(O)** and AUC **(P)** of hypotonic Ca^{2+} responses recorded with 5-BDBD (10μM) or its vehicle. ****, p< 0.0001 (unpaired *t*-test).

Q, Peak ∆Ratio of ATP responses recorded with prior incubation of 5-BDBD (10μM). ****, p<0.0001 (unpaired *t*-test).

Figure 3. Piezo1 is expressed and functional in mouse cholangiocytes

A, Hypotonic Ca^{2+} responses of DIV5 cholangiocytes treated (red trace) or not (black trace) with Gd^{3+} (50μM). Note that Gd^{3+} reduces the amplitude of the hypotonic Ca^{2+} response and converts the response into spike-like signal.

B, Percentage of cholangiocytes showing hypotonic Ca^{2+} responses in the presence of Gd^{3+} (50μM). ****, p< 0.0001 (Fisher test).

C,D, Peak ∆Ratio **(C)** and AUC **(D)** of hypotonic Ca^{2+} responses recorded in the presence of Gd^{3+} (50μM). **, p=0.0042 (**C**) and p=0.0018 (**D**) (unpaired *t*-test).

E, Immunostaining for Piezo1 in HEK.P1KO cells transfected with *GFP-mpiezo1* cDNA (top panels) and in DIV5 mouse cholangiocytes (bottom panels).

F, RT-PCR for mpiezo1 in DIV5 cholangiocytes. Black dot indicate 500 bp DNA marker.

G, Ca^{2+} signals of DIV5 cholangiocytes in response to increasing concentrations (10, 50 and 100μM) of Yoda1.

H, Concentration-response profile for Yoda1 in mouse DIV5 cholangiocytes, yielding apparent EC_{50} of 29.37±1.25 µM (n=99-278).

I, Effect of Yoda1 (50µM) in the absence of external calcium. Data averaged over 84 individual cholangiocytes.

J, Ca^{2+} signals in response to Yoda1 (50 and 100µM) in HEK.P1KO cells transfected with pIRES2-AcGFP1-PIEZO1 or pGFP cDNAs (100µM Yoda1). Traces are mean ± S.E.M. of 60 individual responses per condition.

K, Peak ∆Ratio of Yoda1 responses in HEK.P1KO cells transfected with pIRES2-AcGFP1-PIEZO1 or pGFP cDNAs.

Figure 4. Piezo1 contributes to hypotonic stress-induced Ca^{2+} signals in cholangiocytes

A, Quantitative real-time PCR analysis of the efficiency of *piezo1*-siRNA. Relative levels of piezo1 mRNA in cholangiocytes normalized to the housekeeping genes β-actin, GAPDH and CK19. Data are presented as mean ± S.E.M. based from cholangiocytes transfected with *piezo1*- or scramble-siRNAs (siCtr).

B, Yoda1-induced Ca^{2+} responses recorded in DIV5 cholangiocytes 96h after transfection with scramble-siRNA (siCtr, black trace) or siPiezo1 (red trace).

C, **D**, Percentage of cholangiocytes showing Yoda1-induced Ca^{2+} responses (**C**) and corresponding peak amplitude (**D**) after transfection with siCTR or siPiezo1. ****, p< 0.0001, Fisher test (**C**) and unpaired *t*-test (**D**).

E, Hypotonic Ca^{2+} responses recorded in DIV5 cholangiocytes 96h after transfection with siCtr (black trace) or siPiezo1 (red trace).

F, Percentage of cholangiocytes showing hypotonic Ca^{2+} responses 96h after transfection with siCtr or siPiezo1. **, p= 0.0031, Fisher test.

G-H, Peak ∆Ratio **(G)** and AUC **(H)** of hypotonic Ca^{2+} responses recorded after 96h transfection with siCtr or siPiezo1. ****, p< 0.0001, unpaired *t*-test.

I, Hypotonic Ca^{2+} responses in HEK.P1KO cells transfected with GFP cDNA (black trace) or pIRES2-AcGFP1-PIEZO1 cDNA (red trace). Data shown are mean ± S.E.M. for 52 and 36 cells, respectively.

J,K, Peak ∆Ratio of hypotonic responses (**J**) and ATP (150 µM) responses (**K**) in HEK.P1KO cells transfected with GFP or pIRES2-AcGFP1-PIEZO1 cDNAs. ****, p<0.0001; ns, p=0.4124, unpaired *t*-test.

Figure 5. Piezo1 contributes to hypotonic shock-induced ATP secretion

A, ATP release induced by hypotonic shock in DIV5 cholangiocytes in the presence of Gd^{3+} (100µM) or GsMTx4 (5µM). Data represent means ± S.E.M. for 5-6 separate experiments. *, p=0.0176; **, p= 0.0012; ****, p<0.0001; two way Anova followed by Dunnett's Multiple Comparison test.

B, ATP release induced by hypotonic shock in DIV5 cholangiocytes after 96h transfection with siCtr or siPiezo1. Data from 9 independent experiments normalized to non-stimulated sister cultures. ****, p< 0.0001, one way Anova, Dunnett's multiple comparison test; **, p = 0.01 unpaired *t*-test.

C, Yoda1 (50µM)-induced Ca^{2+} response averaged (± S.E.M) over 110 individual DIV5 cholangiocytes. Note the biphasic shape of the Ca^{2+} response with an initial Ca^{2+} rise (arrowhead) followed by a delayed component (arrow).

D, Representative Yoda1 (50µM)-induced Ca^{2+} responses in the absence (black trace) or presence of apyrase (5U/mL) (red trace).

E,**F**, Proportion of cholangiocytes showing Yoda1-induced Ca^{2+} responses in the presence or absence of apyrase (**E**) and corresponding amplitude of the initial component (**F**). **, p= 0.028 Fisher test, ****, p< 0.0001, unpaired *t*-test.

G, Representative Yoda1 (50µM)-induced Ca^{2+} responses in the presence of apyrase (5U/mL) applied for different durations (10min, black trace; 13min, red trace) after Yoda1 washout. Note the occurrence of a rebound Ca^{2+} component at the apyrase offset.

H, Amplitude of Ca^{2+} rebound occurring at the offset of 10 and 13 min apyrase exposure. Experiments as in (**G**) (N=3).

I,**J** Amplitude of ATP responses as a function of prior exposure to Yoda1 at increasing concentrations. ATP (150µM) was applied 10min after the offset of Yoda1 application (**I**). Each data point in (**J**) shows mean ± S.E.M. from 54-278 cells.

Figure 6. Pannexin1 contributes to hypotonic stress-induced ATP release

A, ATP release induced by hypotonic stress in DIV5 cholangiocytes in the presence of PBC (500µM, 1mM) and CBX (50-100µM). Data represent means ± S.E.M. for 4-9 separate experiments. *, p<0.026; ****, p< 0.0001 (Anova followed by a Dunnett's multiple comparison test).

B, Representative hypotonic Ca^{2+} responses in the presence (red trace) or absence (DMSO, black trace) of PBC (500µM).

C, Percentage of cholangiocytes showing hypotonic Ca^{2+} responses in the presence or absence of PBC. ****, p< 0.0001 (Fisher test).

D-E, Peak ∆Ratio **(D)** and AUC **(E)** of hypotonic Ca^{2+} responses recorded in the presence of PBC. ****, p< 0.0001 (unpaired *t*-test).

F, Proportion of cholangiocytes showing hypotonic-induced Ca^{2+} responses in the presence or not of CBX. ****, p<0.0001 (unpaired *t*-test).

G, Representative Yoda1 (50µM)-induced Ca^{2+} responses in the absence (black trace) or presence of PBC (500µM, red trace).

H,I, Proportion of cholangiocytes showing Yoda1-induced Ca^{2+} responses (**H**) and corresponding peak amplitude (**I**) in the presence or not of PBC. **, p=0.0035 (Fisher test) (**H**); ****, p<0.0001 (unpaired *t*-test) (**I**).

J, Yoda1 (50µM)-induced Ca^{2+} responses in HEK.P1KO cells transfected with pIRES2-AcGFP1-PIEZO1 cDNA in the presence (red trace, n=123) or not (black trace, n=115) of PBC (500µM).

K, Peak ΔRatio of Yoda1-induced Ca^{2+} responses recorded in HEK.P1KO cells transfected with pIRES2-AcGFP1-PIEZO1 cDNA with or without PBC. ns, p=0.386 (unpaired *t*-test).

Figure 7. Identification of Pannexin 1 as an interacting protein of Piezo1

A,B Immunoprecipitates from HEK.P1KO cells cotransfected with Piezo1-GFP and Panx1-flag. Protein interaction was analyzed by immunoprecipitation using anti-flag (**A**) and anti-GFP (**B**) antibodies, followed by immunoblots with the indicated antibodies. Six independent experiments. Inputs: blot membranes were stained with Ponceau red to verify appropriate protein transfer and the presence of the heavy chain of antibodies used for IPs.

C, Pull-down was absent using an anti-Ki67 antibody as control for isotype IgG (left panel). Immunoprecipitation of Panx1-flag was absent in HEKP1KO cells transfected with GFP cDNA and mPanx1-flag (right panel).

D, Immunoprecipitates from NMCs with anti-Piezo1 (right) or anti-Ki67 (left) antibodies. Immunoprecipitation was followed by immunoblots with the anti-Panx1 antibody. Three independent experiments. The arrow indicates Panx1.

Figure 8. Piezo1-Panx1 complex model for stretch-induced ATP release in cholangiocytes

Hypotonic stress elevates intracellular calcium in cholangiocytes through a mechanism that depends on Ca^{2+} influx and secreted ATP. The cellular mechanism of regulated ATP release involves sequential activation of Piezo1 and Panx1. By mediating a rise in intracellular Ca^{2+} Piezo1 is responsible for translating membrane stretch into Panx1-mediated ATP secretion. Released ATP binds P2X4R in an autocrine/paracrine manner, which may influence transport processes and ductal bile secretion.

Figure 1

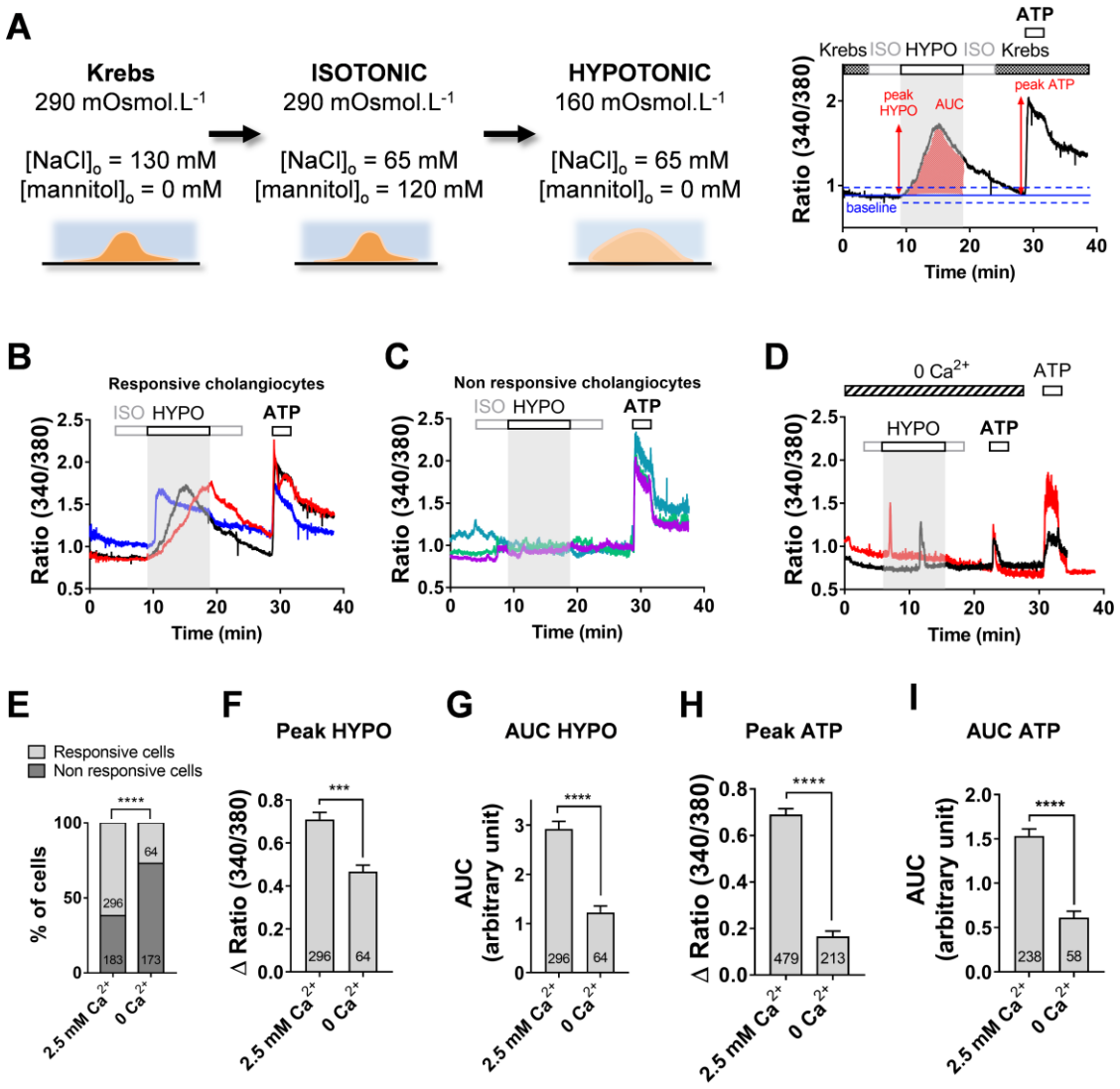
A
Krebs
290 mOsmol.L-1
[NaCl]o = 130 mM
[mannitol]o = 0 mM
ISOTONIC
290 mOsmol.L-1
[NaCl]o = 65 mM
[mannitol]o = 0 mM
HYPOTONIC
160 mOsmol.L-1
[NaCl]o = 65 mM
[mannitol]o = 0 mM
ATP
Krebs ISO HYPO ISO Krebs
peak HYPO
AUC
peak ATP
baseline
Ratio (340/380)
Time (min)
B
Responsive cholangiocytes
ISO HYPO
ATP
C
Non responsive cholangiocytes
D
0 Ca2+
E
Responsive cells
Non responsive cells
% of cells
2.5 mM Ca2+
0 Ca2+
F
Peak HYPO
Δ Ratio (340/380)
G
AUC HYPO
AUC (arbitrary unit)
H
Peak ATP
I
AUC ATP

Figure 2

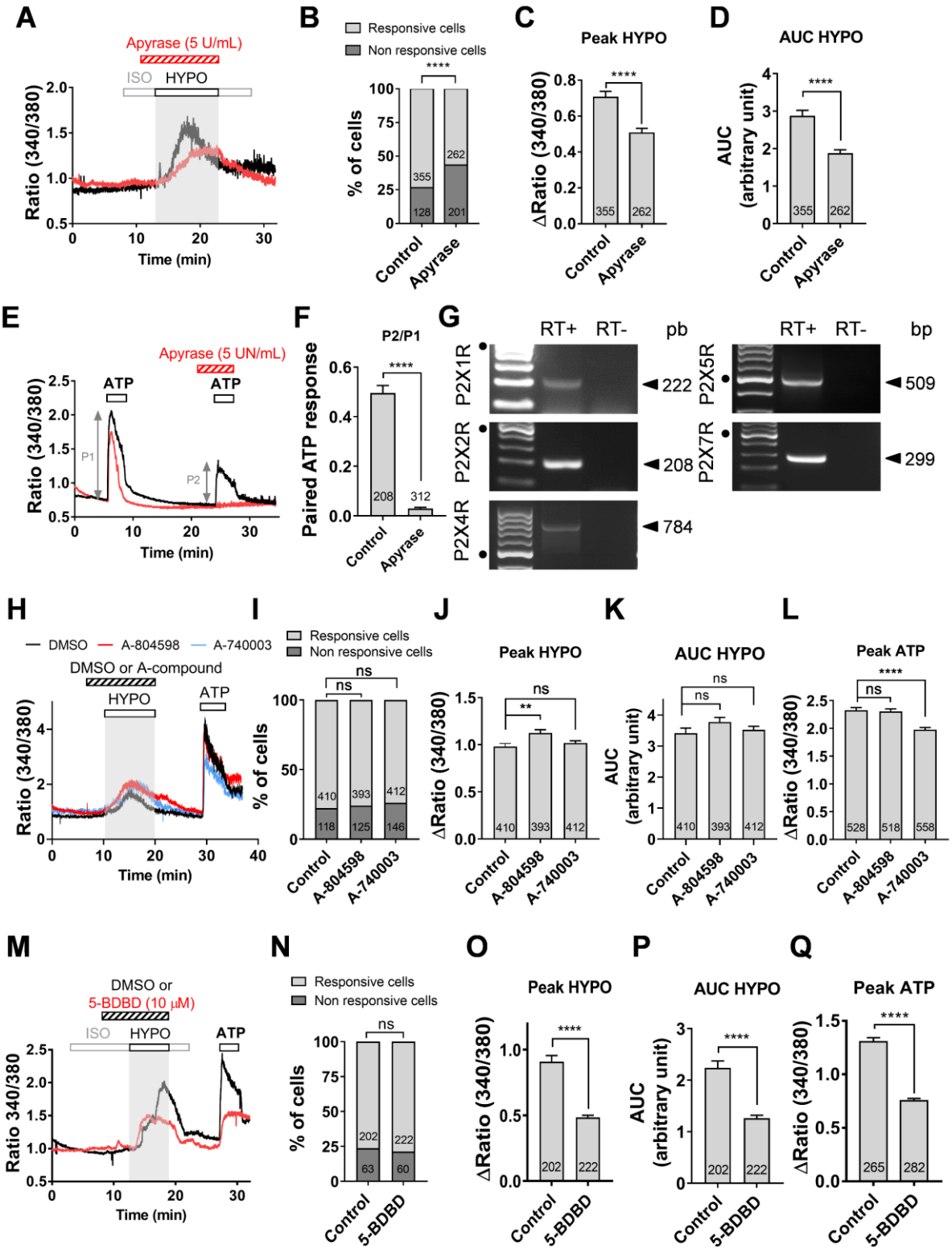
A
Apyrase (5 U/mL)
ISO
HYPO
Ratio (340/380)
Time (min)
B
Responsive cells
Non responsive cells
% of cells
355
128
262
201
Control
Apyrase
C
Peak HYPO
ΔRatio (340/380)
D
AUC HYPO
AUC (arbitrary unit)
E
Apyrase (5 UN/mL)
ATP
P1
P2
F
P2/P1
Paired ATP response
G
RT+
RT-
pb
bp
P2X1R
P2X2R
P2X4R
P2X5R
P2X7R
222
208
784
509
299
H
DMSO
A-804598
A-740003
DMSO or A-compound
HYPO
I
ns
J
Peak HYPO
K
AUC HYPO
L
Peak ATP
M
DMSO or
5-BDBD (10 μM)
Ratio 340/380
N
O
P
Q

Figure 3

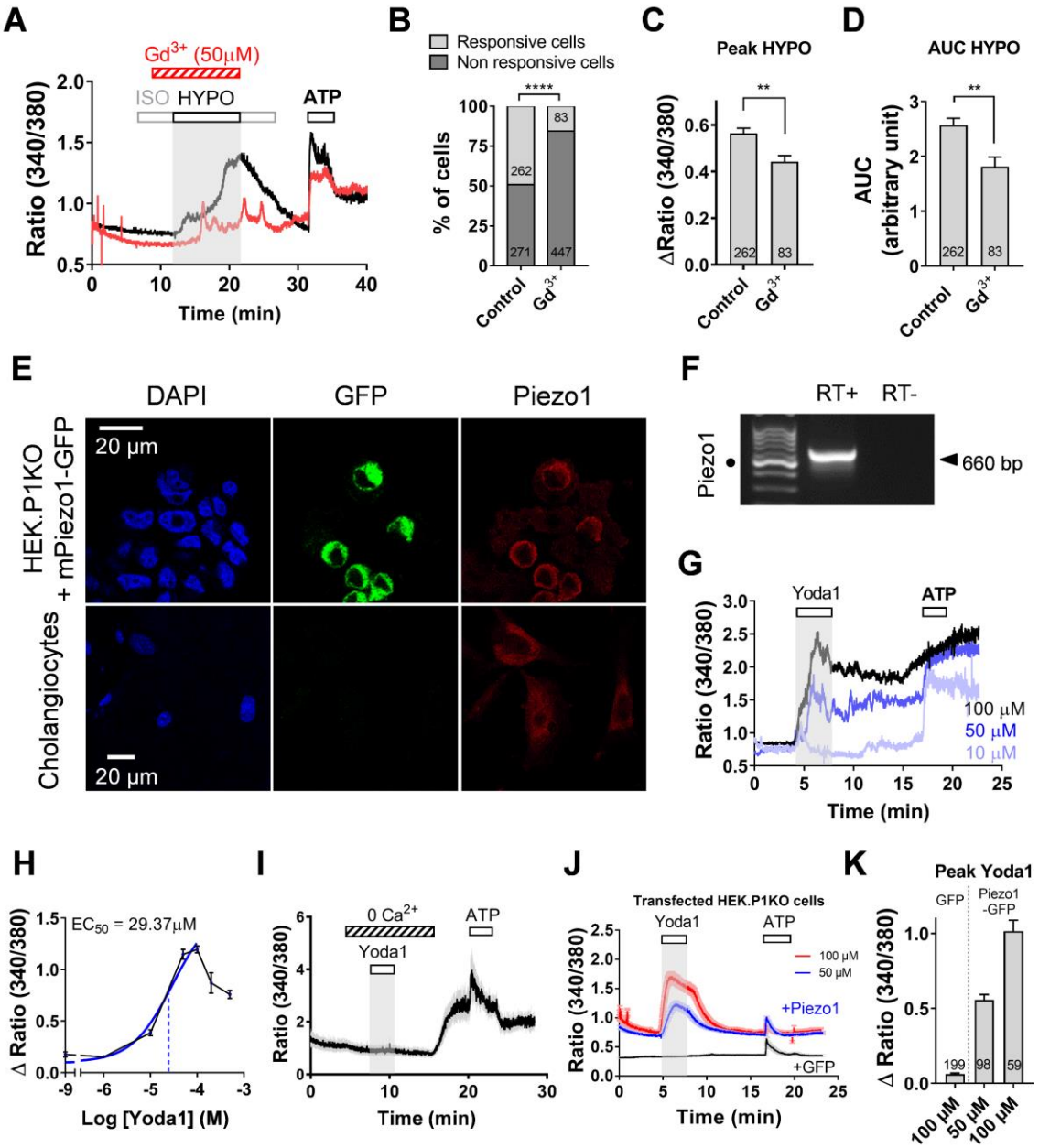
A
Gd3+ (50µM)
ISO HYPO
ATP
Ratio (340/380)
Time (min)
B
Responsive cells
Non responsive cells
****
% of cells
262
271
83
447
Control
Gd3+
C
Peak HYPO
**
ΔRatio (340/380)
262
83
Control
Gd3+
D
AUC HYPO
**
AUC (arbitrary unit)
262
83
Control
Gd3+
E
DAPI
GFP
Piezo1
HEK.P1KO + mPiezo1-GFP
Cholangiocytes
20 µm
20 µm
F
RT+
RT-
Piezo1
660 bp
G
Yoda1
ATP
Ratio (340/380)
100 µM
50 µM
10 µM
Time (min)
H
EC50 = 29.37µM
Δ Ratio (340/380)
Log [Yoda1] (M)
I
0 Ca2+
Yoda1
ATP
Ratio (340/380)
Time (min)
J
Transfected HEK.P1KO cells
Yoda1
ATP
100 µM
50 µM
+Piezo1
+GFP
Ratio (340/380)
Time (min)
K
Peak Yoda1
GFP
Piezo1 -GFP
Δ Ratio (340/380)
199
98
59
100 µM
50 µM
100 µM

Figure 4

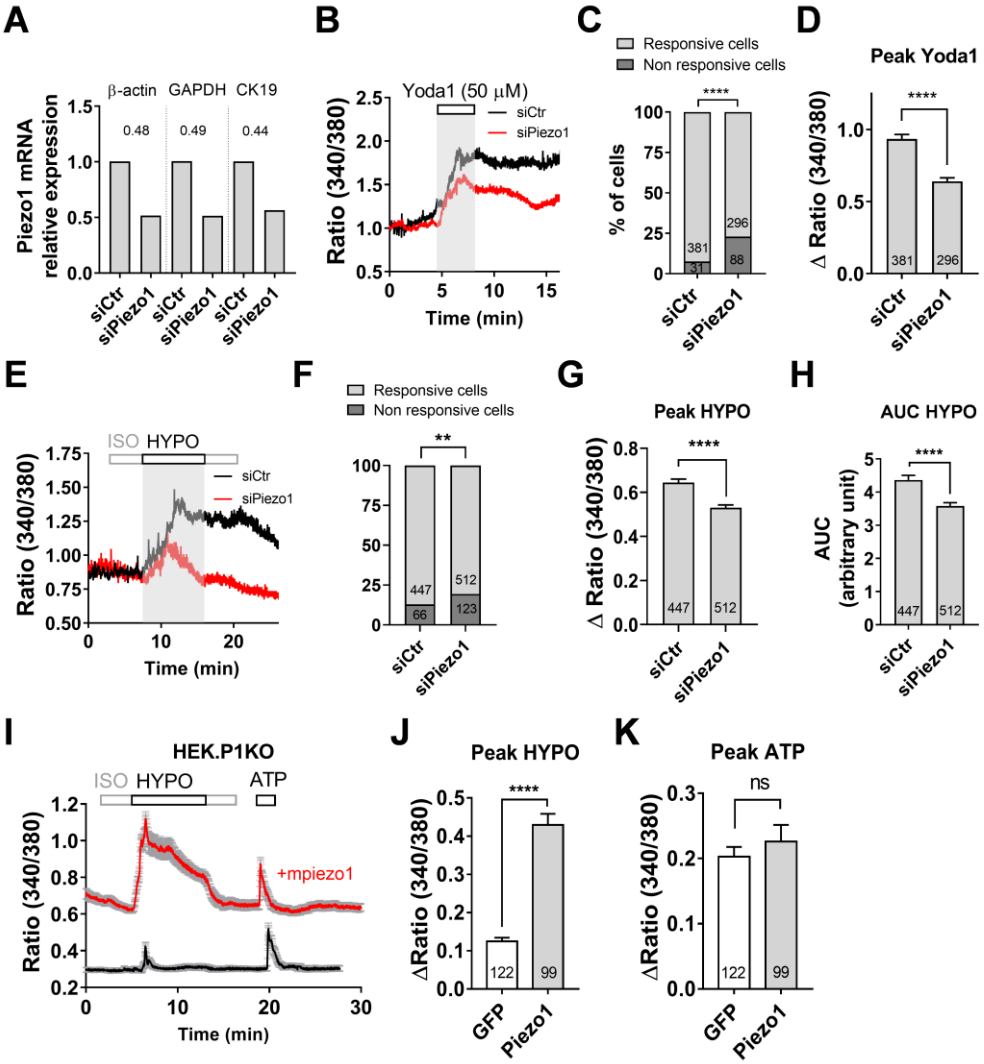
A
β-actin GAPDH CK19
0.48
0.49
0.44
Piezo1 mRNA relative expression
siCtr siPiezo1 siCtr siPiezo1 siCtr siPiezo1
B
Yoda1 (50 μM)
siCtr
siPiezo1
Ratio (340/380)
Time (min)
C
Responsive cells
Non responsive cells
****
% of cells
381
31
296
88
siCtr siPiezo1
D
Peak Yoda1
****
Δ Ratio (340/380)
381
296
siCtr siPiezo1
E
ISO HYPO
siCtr
siPiezo1
Ratio (340/380)
Time (min)
F
Responsive cells
Non responsive cells
**
447
66
512
123
siCtr siPiezo1
G
Peak HYPO
****
Δ Ratio (340/380)
447
512
siCtr siPiezo1
H
AUC HYPO
****
AUC (arbitrary unit)
447
512
siCtr siPiezo1
I
HEK.P1KO
ISO HYPO
ATP
+mpiezo1
Ratio (340/380)
Time (min)
J
Peak HYPO
****
ΔRatio (340/380)
122
99
GFP Piezo1
K
Peak ATP
ns
ΔRatio (340/380)
122
99
GFP Piezo1

Figure 5

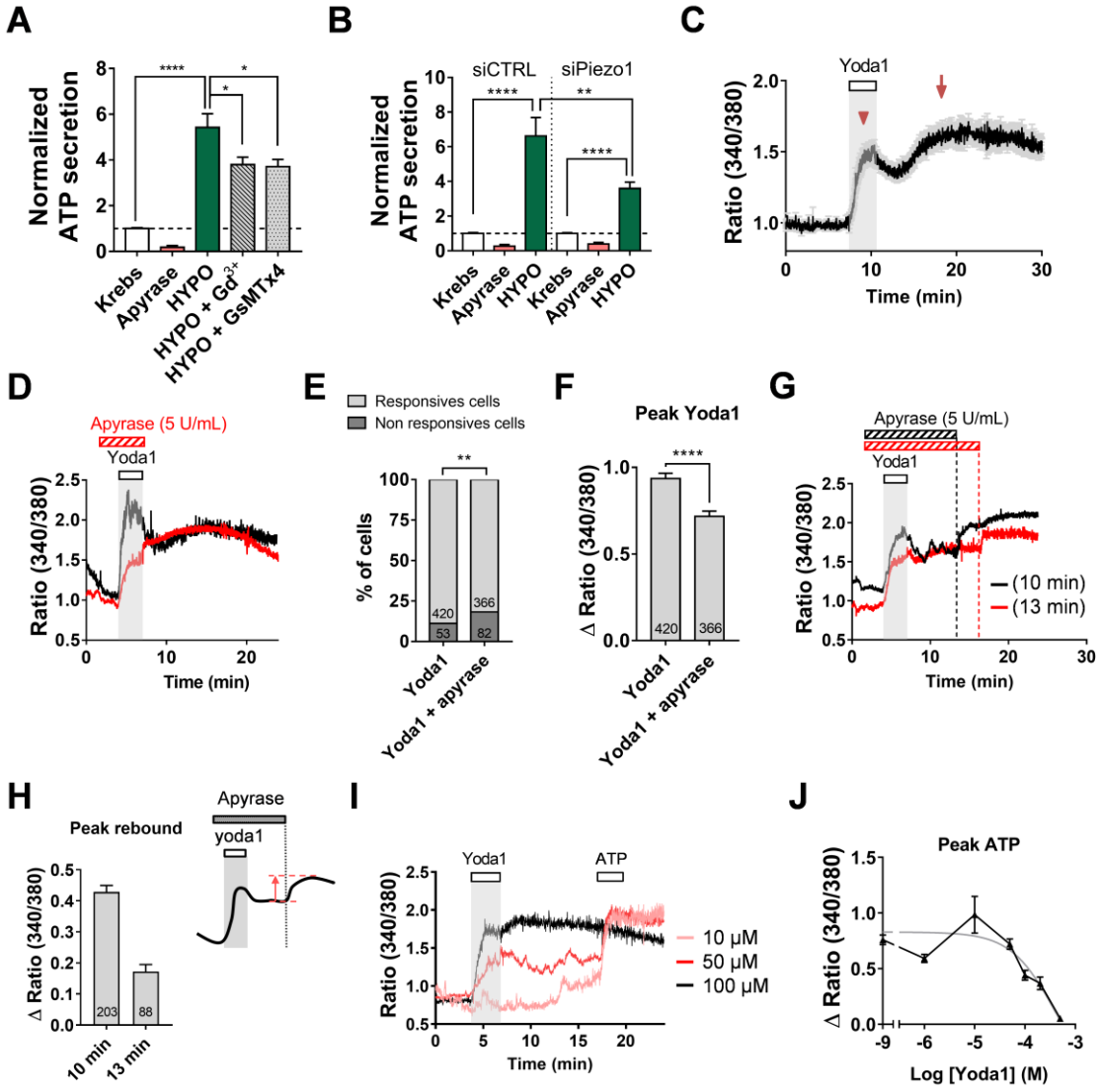
A
Normalized ATP secretion
Krebs
Apyrase
HYPO
HYPO + Gd3+
HYPO + GsMTx4
B
siCTRL
siPiezo1
Normalized ATP secretion
Krebs
Apyrase
HYPO
Krebs
Apyrase
HYPO
C
Yoda1
Ratio (340/380)
Time (min)
D
Apyrase (5 U/mL)
Yoda1
Ratio (340/380)
Time (min)
E
Responsives cells
Non responsives cells
% of cells
420
53
366
82
Yoda1
Yoda1 + apyrase
F
Peak Yoda1
Δ Ratio (340/380)
420
366
Yoda1
Yoda1 + apyrase
G
Apyrase (5 U/mL)
Yoda1
Ratio (340/380)
(10 min)
(13 min)
Time (min)
H
Peak rebound
Apyrase
yoda1
Δ Ratio (340/380)
203
88
10 min
13 min
I
Yoda1
ATP
Ratio (340/380)
10 µM
50 µM
100 µM
Time (min)
J
Peak ATP
Δ Ratio (340/380)
Log [Yoda1] (M)

Figure 6

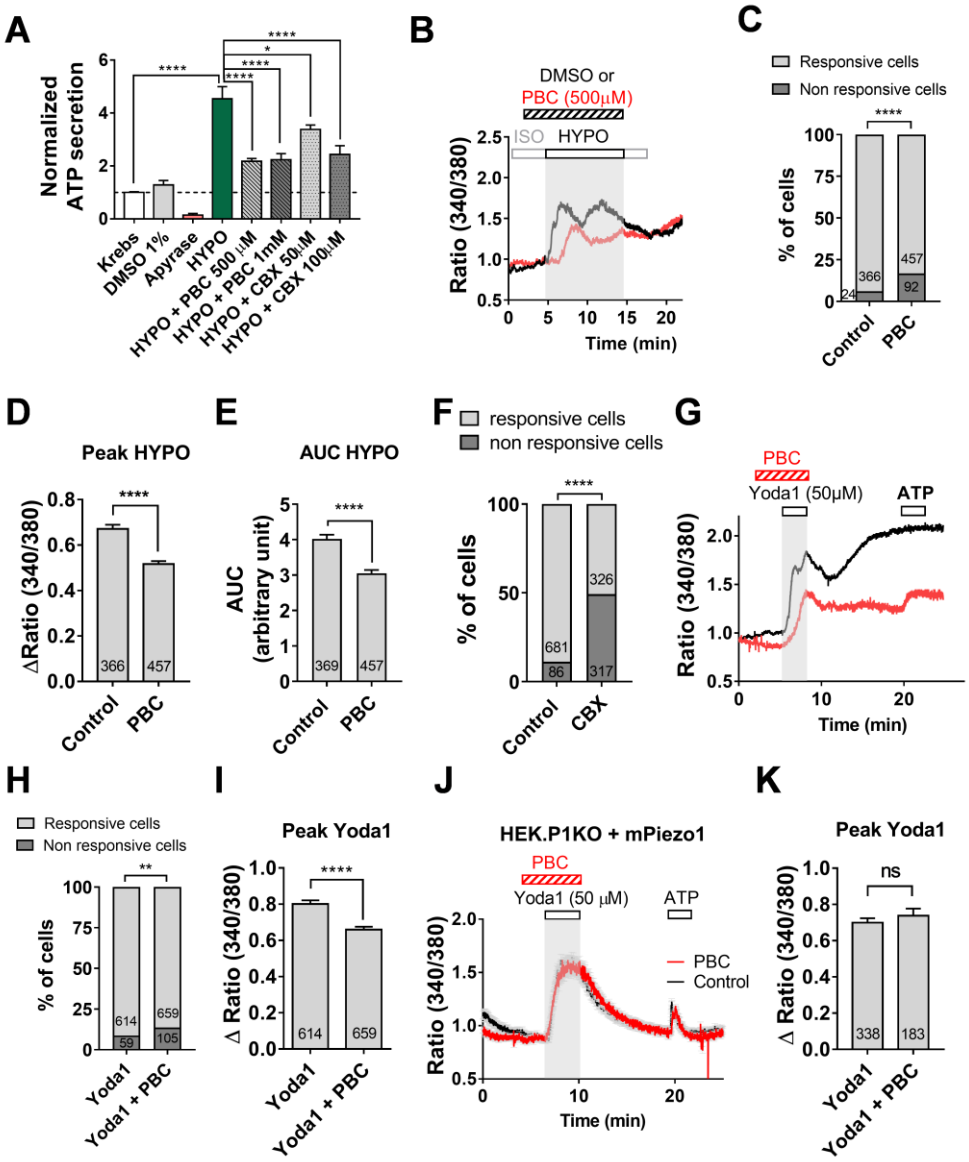
A
Normalized ATP secretion
Krebs
DMSO 1%
Apyrase
HYPO
HYPO + PBC 500 µM
HYPO + PBC 1mM
HYPO + CBX 50µM
HYPO + CBX 100µM
B
DMSO or
PBC (500µM)
ISO
HYPO
Ratio (340/380)
Time (min)
C
Responsive cells
Non responsive cells
% of cells
Control
PBC
D
Peak HYPO
ΔRatio (340/380)
E
AUC HYPO
AUC (arbitrary unit)
F
responsive cells
non responsive cells
% of cells
Control
CBX
G
PBC
Yoda1 (50µM)
ATP
Ratio (340/380)
Time (min)
H
Responsive cells
Non responsive cells
% of cells
Yoda1
Yoda1 + PBC
I
Peak Yoda1
Δ Ratio (340/380)
J
HEK.P1KO + mPiezo1
PBC
Yoda1 (50 µM)
ATP
PBC
Control
Ratio (340/380)
Time (min)
K
Peak Yoda1
ns
Δ Ratio (340/380)

Figure 7

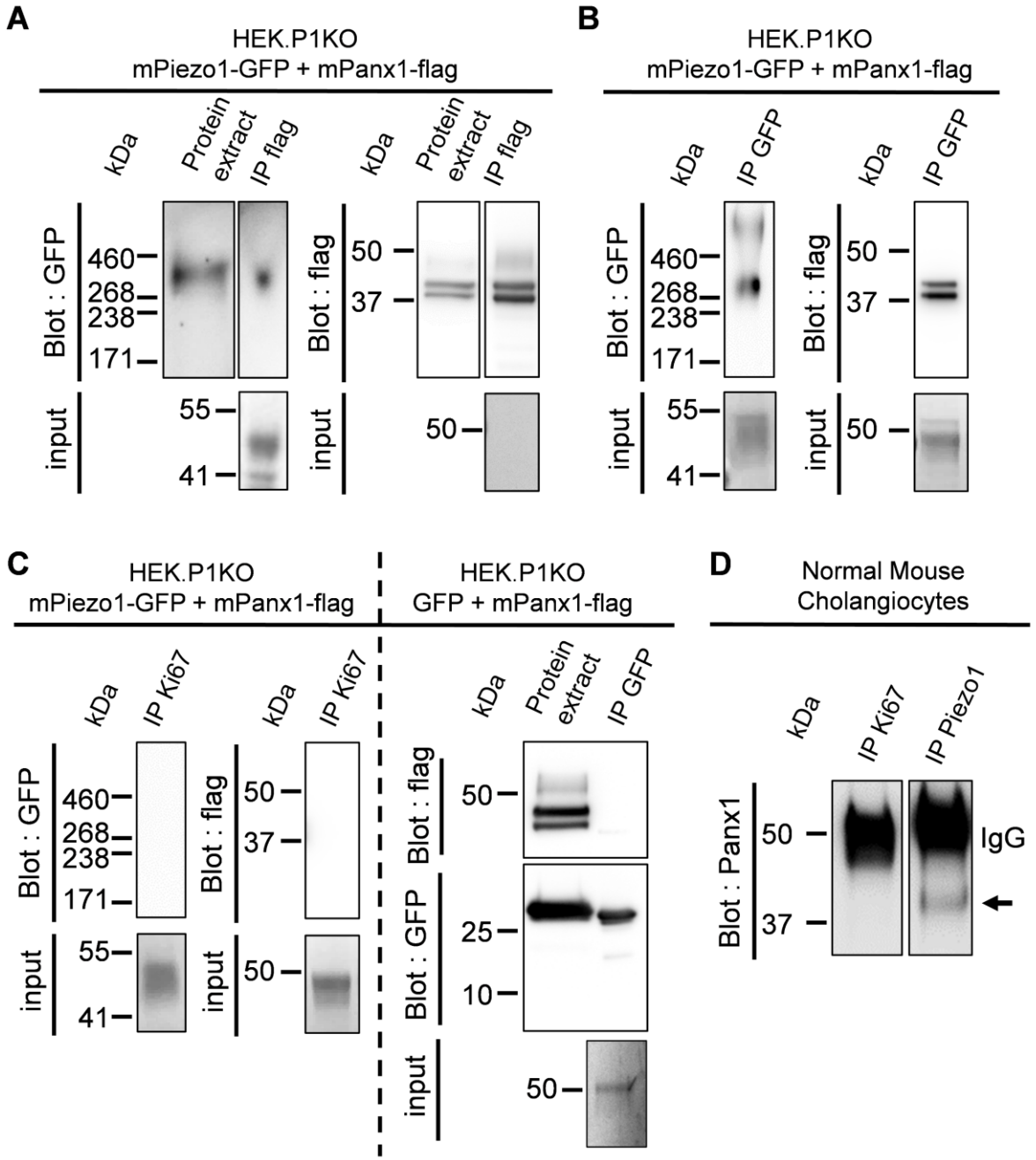
A
HEK.P1KO
mPiezo1-GFP + mPanx1-flag
kDa
Protein extract
IP flag
Blot : GFP
460
268
238
171
input
55
41
Blot : flag
50
37
input
50
B
HEK.P1KO
mPiezo1-GFP + mPanx1-flag
kDa
IP GFP
Blot : GFP
460
268
238
171
input
55
41
Blot : flag
50
37
input
50
C
HEK.P1KO
mPiezo1-GFP + mPanx1-flag
kDa
IP Ki67
Blot : GFP
460
268
238
171
input
55
41
Blot : flag
50
37
input
50
HEK.P1KO
GFP + mPanx1-flag
kDa
Protein extract
IP GFP
Blot : flag
50
Blot : GFP
25
10
input
50
D
Normal Mouse
Cholangiocytes
kDa
IP Ki67
IP Piezo1
Blot : Panx1
50
37
IgG

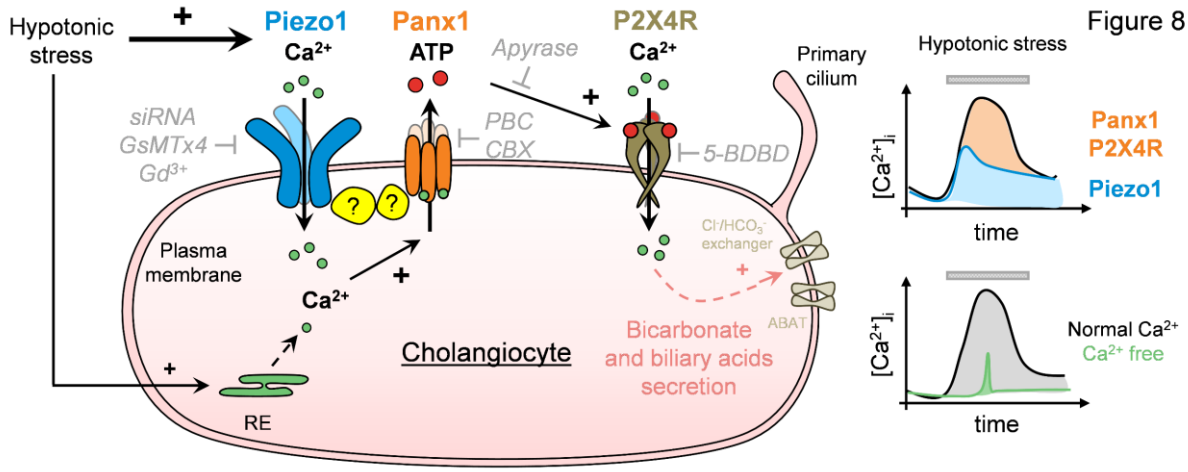
Hypotonic stress
+
Piezo1
Ca2+
Panx1
ATP
Apyrase
P2X4R
Ca2+
Primary cilium
siRNA
GsMTx4
Gd3+
PBC
CBX
5-BDBD
?
?
Plasma membrane
Ca2+
+
Cl-/HCO3- exchanger
ABAT
Bicarbonate and biliary acids secretion
Cholangiocyte
RE
Hypotonic stress
[Ca2+]i
time
Panx1
P2X4R
Piezo1
[Ca2+]i
time
Normal Ca2+
Ca2+ free

Figure 8

Piezo1-Pannexin 1 complex couples force detection to ATP secretion in cholangiocytes

Angélique Desplat[1], Virginie Penalba[1], Emeline Gros[1], Thibaud Parpaite[1], Bertrand Coste[1], Patrick Delmas[1]*

[1]Aix-Marseille-Université, CNRS, Laboratoire de Neurosciences Cognitives, UMR 7291, CS80011, Bd Pierre Dramard, 13344 Marseille, France.

Supplemental Materials and Methods

Gene silencing by siRNA.

	siPiezo1	**siScramble**
Target	GAAAGAGAUGUCACCGCUA	UGGUUUACAUGUCGACUAA
Sequences	GCAUCAACUUCCAUCGCCA	UGGUUUACAUGUUGUGUGA
(5'→ 3')	AAAGACAGAUGAAGCGCAU	UGGUUUACAUGUUUUCUGA
	GGCAGGAUGCAGUGAGCGA	UGGUUUACAUGUUUUCCUA

Supplemental Table 1. Sequences of siRNA.

RT-PCR primers. Specific oligonucleotides were synthesized based on mouse sequences (**Table 2**) and purchased from Eurofins-genomics.

Genes	**Reference no. / Accession no.**	**Forward primer (5'→ 3')**	**Reverse primer (5'→ 3')**	**Size (pb)**
CK-19	NM_008471.3	TTG CTC GGA TTG AGG AGC TG	TTC ATG CTG TGC TGG GAC TG	136

CK-7	NM_033073.3	CTC TCG CTC CAC TGC TTA CC	CGA CTG CAG CTC TGC TAA CT	679
CFTR	NM_021050.2	TGC GAT CTG TGA GCA GAG TG	GCA CAT AAC CCC CAT CCA CA	570
AE2	NM_009207.3	GGT GGA TAG AGA GCG TGA GC	TGT CCT CCG AAG GGG ATC AT	598
ASBT	NM_011388.3	GGC TAC AGC CTG GGT TTC TT	CAC CAG GTT GAG ATC CTC GG	150
Albumin	NM_009654.4	CAG ATG ACA GGG CGG AAC TT	AGG TGC TTT CTG GGT GTA GC	488
Piezo1	NM_001357349.1	GCTTTTGGGAAGCACT CTGC	CACAGAGCGGATCAGTGA CA	660
Piezo1	NM_001142864.4, NM_001357349.1	TTC CCC AAC AGC ACC AAC TT	GGC AGG TAC AGC CAC TTG AT	596
Piezo2	NM_001039485.4	CAG CCA TGC CAA AGT CAA TGG	CCA CTT GTT CCT GAG GTC TGA	277
TRPV2	NM_011706.2	ATG CTT AGA ACT AAG GTG GAG G	AGA GTC GGT CAC GGT CAA AC	498
TRPV4	NM_022017.3	CCT GCT CTT CAT GAT CGG CT	AGA CCA GTT CAC CTC GTC CA	496
PKD1	NM_013630.2	GCA GCT TCA GTG TGG TCT CT	GAA GAT GGC AGC ACT CTG GT	539
PKD2	M_008861.3	TGG AAG TTC ACC GAA GGC TC	AGC CCC TCT TCA TTT GAC AT	767

P2rX1	NM_008771.3	GAC AAA CCG TCG TCA CCT CT	CCC ATG TCC TCC GCA TAC TT	222
P2rX2	NM_001310701.1	TGG ACA GGC AGG GAA ATT CA	CAA GAC AAG GGC AAG GGT CA	208
P2rX4 mouse	NM_011026.3	TGT GGC TGT GAC CAA CAC TT	GTC AAA CTT GCC AGC CTT TCC	784
P2rX4 human	NM_001256796.2	GTCAGCTCCGTTACGA CCAA	CGTCTTGACAGACCCGTTG A	294
P2rX5	NM_033321.3	CCC ACT GCA ACC CAC ACT AT	ATT CTC CTG GAG GCC AGA CC	509
P2rX7	NM_001038839.2	TTA TGG CAC CGT CAA GTG GG	GCC TGG GAT ACT CAG GAC AC	299
Panx1	NM_019482.2	AGA TCT CCA TCG GTA CCC AGA	GTG GGA GGT TTC CAG ACT CG	138

Supplemental Table 2. Sequences of RT-PCR primers.

Real time qPCR. The RQ formula was RQ = $2^{(-\Delta\Delta Ct)}$ with ΔCt the difference between values of *piezo1* and the housekeeping genes and ΔΔCt the difference between the normalized values (ΔΔCt = ΔCt siPiezo1 - ΔCt siCtr).

Transcript	**Reference no. / accession no.**	**Forward primer (5'→ 3')**	**Reverse primer (5'→ 3')**	**Size (pb)**
Piezo1	NM_001357349.1	ATC GCC ATC ATC TGG TTC CC	CTA GCT TGA GGG TGA CGG TG	100

CK-19	NM_008471.3	AAG ACC ATC GAG GAC TTG CG	GCG TGT TCT GTC TCA AAC TTG G	128
GAPDH	XM_017321385.1	GCA AAT TCA ACG GCA CA	CAC CAG TAG ACT CCA CGA C	141
β-actin	NM_007393.5	GCC AAC CGT GAA AAG ATG AC	GGC GTG AGG GAG AGC ATA G	183

Supplemental Table 3. Sequences of qPCR primers.

Immunostaining. After incubation with primary antibodies and three washes with PBS-containing Triton 0.05% TritonX-100, cells were incubated with secondary antibodies (1:1000) at RT for 1h. Secondary antibodies used were as follows: Donkey anti-rabbit IgG coupled to TRITC (Jackson ImmunoResearch); Donkey anti-goat IgG coupled to Alexa 488 (Invitrogen); Donkey anti-mouse IgG coupled to Alexa 488 (Invitrogen). Donkey anti-mouse IgG coupled to Alexa 647 (Invitrogen). Actin filaments were labelled using Phalloidin-FITC (50 µg/mL, Sigma) for 1 h and cell nucleus were stained using DAPI (Sigma) for 10 min. Coverslips were finally washed with Triton 0.05X-containing PBS before being mounted with fluoromount-G mounting media (DAKO). Images were acquired using an inverted epifluorescence microscope (Axio Observer Z1 Zeiss) processed with Axovision software (Zeiss) or a Zeiss LSM780 laser scanning microscope, using Zen Software. Images were later exported into Image J software for final processing. Negative controls (i.e. secondary antibodies alone, no primary antibodies) were performed in all experiments and showed no staining.

Immunoprecipitation from transfected HEK.P1KO cells. Proteins from HEK.P1KO cells transiently transfected with a given construct (mPiezo1-GFP, mPannexin1-flag, GFPsparck) were extracted using a buffer containing 25 mM Hepes, 150 mM NaCl, 15 mM EDTA, 20 mM N-Ethylmaleimide (Sigma #E3876), 1.2% TritonX-100 and a cocktail of protease inhibitors (Roche #04 693 116 001). Cell lysates were then rotated for 30 min and centrifuged at 10.000 g for 20 min at 4°C.

Western Blot. To display Piezo1-GFP protein, protein samples were loaded in 3-8% precasted polyacrylamide gel (Invitrogen). Proteins were blotted on a nitrocellulose membrane in transfer buffer containing 20% methanol at 33V overnight at 4°C. To display Panx1-flag protein, western blots were performed using 4-12% precasted polyacrylamide gel (ThermoFisher Scientific) and the transfer was done in buffer containing 10% 2-propanol at 250 mA for 2 h and 30 min at RT.

Mass Spectrometry. After elution from the beads, proteins were trapped in acrylamide gel using the so-called tube-gel method and digested with trypsin (200 ng) overnight at 37°C. Protein samples were analyzed by mass spectrometry using a hybrid Q-Orbitrap mass spectrometer (Q-Exactive, Thermo Fisher Scientific, United States) coupled to a nanoliquid chromatography (LC) Dionex RSLC Ultimate 3000 system (Thermo Fisher Scientific, United States). Fragmentation spectra of the 10 most abundant peaks (Top10 method) were acquired with high-energy collision dissociation (HCD) at a normalized collision energy of 27%. All raw data files were processed to generate .mgf files and searched against the Swissprot database (taxonomy: mus musculus) using the MASCOT software (www.matrixscience.com). Search parameters were as follows: variable modifications, methionine oxidation, mass tolerance, 10 ppm on parent ion and 0.02Da on fragment ions, and a maximum of two tryptic missed cleavages.

Supplemental Figure legends

Supplemental Figure 1. Mouse cholangiocytes in primary culture are not sensitive to hypertonic stress

A, Cultured cells from mouse IBDUs were co-labelled at DIV5 with an antibody against the cholangiocyte marker CK19 (red) and an antibody against the hepatocyte marker albumin (green). The cell nucleus is stained with DAPI (blue) to allow cell counting. Note that all cells reactive to the CK19 antibody (asterisks) are negative for albumin. The arrow indicates a cell negative to both CK19 and albumin, possibly a fibroblast. Inset: a rare albumin-positive cell seen in mouse IBDU cultures at DIV5.

B, Percentage of CK19-positive cells in mouse IBDU cultures. Data normalized to the number of DAPI-positive cells (indicated on each bar).

C, IBDU cultures at DIV5 express the typical cholangiocyte markers CK19, CK7, ASBT, CFTR and AE2a at mRNA level. Black dots indicate 500 bp DNA marker, each band are separated by 100 bp.

D, Effects of an hypertonic solution (460 mOsmol.L^{-1}) on DIV5 cholangiocytes. Data points are mean ± S.E.M. (n=26). ATP (150 µM) was applied at the end of the experiment to probe cell viability.

E, Ratiometric values determined before (Krebs) and after (Hyper) exposure to the hypertonic solution. Note that ATP (150 µM) caused normal Ca^{2+} mobilization in cells insensitive to the hypertonic solution. ns, not significant (p= 0.5029), paired *t*-test.

Supplemental Figure 2. **The primary cilium is not involved in osmosensation**

A, CK19-positive DIV5 cholangiocytes stained with acetylated-tubulin in cultures. Primary cilia are indicated by arrows. The confocal image z-stacks spanned 0.33 µm. Upper panels: three-dimensional reconstruction pointing out primary cilia (arrowheads).

B, Percentage of ciliated CK19-positive cholangiocytes in mouse IBDU cultures at different times *in vitro*. The total number of analyzed CK19-positive cells is indicated on each bar.

C, Cholangiocytes stained with acetylated-tubulin in cultures treated with chloral hydrate (4 mM, 24h).

D, Percentage of CK19-expressing cells in DIV5 IBDU cultures treated or not with chloral hydrate. *, p= 0.044, Fisher test.

E, Chloral hydrate treatment reduces the percentage of ciliated cells amongst the CK19-expressing cells. **** p<0.0001, Fisher test.

F, Hypotonic shock-induced Ca^{2+} responses in cholangiocytes pre-treated with chloral hydrate (4 mM) (red trace) or with the vehicle (black trace).

G, Percentage of responsive cholangiocytes in control and chloral hydrate conditions. ns, not significant (p= 0.5378, Fisher test).

H, Peak amplitude of hypotonic Ca^{2+} responses in control and chloral hydrate conditions. ns, not significant (p= 0.4445, *t*-test).

I, Peak ΔRatio of ATP (150 µM) responses in cholangiocytes from control and chloral hydrate-treated IBDU cultures. ****, p<0.0001 (unpaired *t*-test).

J, Hypotonic shock-induced Ca^{2+} responses in cholangiocytes pre-treated with suramin (20 µM) (red trace) or with the vehicle (black trace).

K, Peak amplitude of hypotonic Ca^{2+} responses in control and suramin conditions (20 and 200 µM). ***, p<0.001 (unpaired *t*-test); ns, not significant (p = 0.34; unpaired t-test).

Supplemental Figure 3. **Expression of putative mechanosensitive channels in cholangiocytes**

A, Typical ethidium bromide-stained gels of RT-PCR products from DIV5 cholangiocyte RNA extracts, demonstrating the presence of TRPV2, TRPV4, TRPP1, TRPP2, Piezo1 and Piezo2. Size markers are shown in the left lanes. Black dots indicate the 500 bp DNA marker.

B, Identification of Piezo 1 by mass spectrometry in cholangiocytes. Piezo1 protein was identified with a sequence coverage of 10%. The identified peptides from mpiezo1 (https://db.systemsbiology.net/sbeams/cgi/PeptideAtlas; E2JF22) are shown in blue, and their position on Piezo1 sequence indicated in column one. Experimental peptide ions m/z (mass to charge ratios), experimental and theoretical peptide masses, experimental error (in ppm), trypsin misscleavages, peptide sequence and modifications are also indicated. (C) Carbamidomethyl; (M) Oxidation.

Supplemental Figure 4. Yoda1 does not induce ATP secretion by itself

A, Apyrase did not reduce Yoda1 (50 µM)-induced Ca^{2+} responses in piezo1-GFP-transfected HEK P1KO cells. Data averaged from 115 cells in the two conditions.

B, Peak amplitude of Yoda1-induced Ca^{2+} responses in piezo1-GFP-transfected HEKP1KO cells with and without apyrase.

C, P2X4R is detected by RT-PCR in native, untransfected HEKP1KO cells. Black dot indicates the 500 bp DNA marker. Data from triplicates.

D, Lack of effect of Yoda1 (100 µM) on ATP secretion in HEK293T and HEKP1KO cells. Data are mean ± S.E.M. from triplicates. $\text{Normalized } [\text{ATP}] = \frac{(\text{ODkrebs} - \text{ODblank})}{\text{ODkrebs} - \text{ODblank}}$

E, Lack of effect of Yoda1 on ATP secretion in HEKP1KO cells overexpressing Piezo1-GFP. Data from triplicates.

Supplemental Figure 5. **Panx1 co-localizes with Piezo1 in cholangiocyte plasma membrane**

A, RT-PCR for Panx1 in DIV5 cholangiocytes and Normal Mouse Cholangiocytes (NMCs). Black dots indicate the 500 bp DNA marker.

B, Anti-Flag and anti-Panx1 immunostainings in DIV5 cholangiocytes (bottom) and in HEKP1KO cells transfected with Flag-panx1 cDNA (top).

C, Western blot analysis of Panx1 expression in whole cell lysates from HEKP1KO cells expressing Panx1-Flag (left panel), cholangiocytes (middle panel) and NMCs (right panel).

D, Immunofluorescent staining of Piezo1-GFP and Pannexin1-flag overexpressed in HEK.P1KO cells. Cells were labeled using an Alexa647-coupled anti-flag (shown in green) and a TRITC-coupled anti-GFP (shown in red).

E, The line scan illustrates overlap of Piezo1-GFP and Panx1-flag labels at the cell periphery.

Supplemental Figure 6. Reconstitution of Piezo1/Panx1/P2X4R mechanosecretory pathway in HEK cells

A, Triple immunofluorescent stainings in a HEK.P1KO cell transfected with Piezo1-GFP, Panx1-HA and P2X4R-myc.

B, Ca^{2+} signals in response to Yoda1 (50 µM) in HEK.P1KO cells transfected with GFP (green trace), Piezo1-GFP and DsRed (black trace), Piezo1-GFP, Panx1 and DsRed (blue trace) and Piezo1-GFP, Panx1 and P2X4R (red trace). The ratio of cDNA is indicated in brackets. Note the huge increase in the purinergic response in the cell expressing P2X4R.

C, Peak amplitude of Yoda1-induced Ca^{2+} responses in transfected HEK.P1KO cells as indicated. *, p = 0.0479; **, p = 0.0029; *** p = 0.0005 (unpaired t-test). N = 2.

D, Yoda1-induced Ca^{2+} responses in HEK.P1KO cells expressing Piezo-GFP and DsRed (black trace) or Piezo-GFP, Panx1 and P2X4R (red trace) and treated with apyrase (5 U/mL). Note the overshoot response when apyrase was turned off.

Supplemental Table 4.

Detailed information depicting the numbers of independent experiments (N), the number of cells (n) analyzed in each individual experiment and the corresponding averaged values. Units are not reported and can be found in the figures.

Figure panels		Independent tests (N)	Conditions	Number of cells (n) in each N and corresponding mean value or % of responsive cells
1	E	5	2.5 mM Ca^{2+}	n = 59, 77, 71, 137, 135 % = 98.3, 85.71, 78.87, 59.85, 25.18
			0 Ca^{2+}	n total = 24, 41, 40, 52, 80 % = 25.00, 73.17, 30.00, 15.38, 10.00
	F	5	2.5 mM Ca^{2+}	n = 58, 66, 56, 82, 34 mean = 1.02, 0.97, 0.61, 0.47, 0.42
			0 Ca^{2+}	n = 6, 30, 12, 8, 8 mean = 0.32, 0.55, 0.51, 0.27, 0.35
	G	5	2.5 mM Ca^{2+}	n as in F mean = 4.07, 3.81, 2.74, 2.10, 1.47
			0 Ca^{2+}	n as in F mean = 1.39, 1.22, 1.57, 0.62, 1.14
	H	4	2.5 mM Ca^{2+}	n = 66, 56, 82, 34 mean = 1.45, 0.47, 0.24, 0.88, 0.90
			0 Ca^{2+}	n = 30, 12, 8, 8 mean = 0.29, 0.34, 0.04, 0.21
	I	4	2.5 mM Ca^{2+}	n as in H mean = 2.64, 0.99, 0.88, 1.85
			0 Ca^{2+}	n as in H mean = 0.61, 0.84, 0.16, 0.73
2	B	3	Ctrl	n = 197, 139, 147 % = 67.01, 94.96, 61.90
			Apyrase	n = 52, 287, 124 % = 46.15, 60.63, 51.61
	C	3	Ctrl	n = 92, 131, 132 mean = 0.67, 0.87, 0.56
			Apyrase	n = 64, 174, 24

				mean = 0.47, 0.54, 0.28
	D	3	Ctrl	n as in C mean = 2.68, 3.37, 2.54
			Apyrase	n as in C mean = 1.59, 2.08, 1.19
	F	3	Ctrl	n = 81, 66, 61 mean = 0.47, 0.41, 0.63
		3	Apyrase	n = 119, 79, 114 mean = 0.02, 0.01, 0.06
	I	3	Ctrl	n = 173, 164, 191 % = 87.86, 59.15, 84.29
		4	A-804598	n = 186, 130, 96, 106 % = 75.27, 69.23, 75.00, 85.84
		4	A-740003	n = 216, 172, 85, 85 % = 79.17, 60.47, 83.53, 77.65
	J	3	Ctrl	n = 152, 97, 161 mean = 0.90, 1.07, 1.00
		4	A-804598	n = 140, 90, 72, 91 mean = 1.13, 0.94, 1.12, 1.30
		4	A-740003	n = 171, 104, 71, 66 mean = 1.17, 0.93, 1.09, 0.66
	K	3	Ctrl	n as in J mean = 3.42, 2.98, 3.76
		4	A-804598	n as in J mean = 3.68, 3.54, 2.71, 4.96
		4		n as in J

			A-740003	mean = 4.20, 3.49, 3.53, 2.13
	L	3	Ctrl	n as in I mean = 2.15, 1.91, 2.86
		4	A-804598	n as in I mean = 1.97, 2.26, 1.95, 3.28
		4	A-740003	n as in I mean = 1.81, 1.97, 2.16, 2.27
	N	3	Ctrl	n = 86, 105, 74 % = 97.67, 75.24, 52.70
		3	5-BDBD	n = 98, 115, 69 % = 88.78, 83.47, 56.52
	O	3	Ctrl	n = 83, 79, 39 mean = 1.12, 0.74, 0.81
			5-BDBD	n = 87, 96, 39 mean = 0.51, 0.46, 0.45
	P	3	Ctrl	n as in O mean = 3.57, 1.39, 1.09
			5-BDBD	n as in O mean = 1.08, 1.43, 1.23
	Q	3	Ctrl	n as in N mean = 1.50, 1.22, 1.19
		3	5-BDBD	n as in N mean = 0.67, 0.74, 0.89
3	B	3	Ctrl	n = 245, 125, 163 % = 69.79, 38.40, 26.38
			Gd^{3+}	n = 246, 156, 128

				% = 18.29, 14.10, 12.50
	C	3	Ctrl	n = 171, 48, 43 mean = 0.61, 0.47, 0.48
			Gd^{3+}	n = 45, 22, 16 mean = 0.47, 0.38, 0.47
	D	3	Ctrl	n as in C mean = 3.05, 1.81, 1.55
			Gd^{3+}	n as in C mean = 3, 2.08, 1.27, 1.50
	H	2	10 µM	n = 136, 67 mean = 0.33, 0.49
			50 µM	n = 130, 148 mean = 1.42, 0.91
			100 µM	n = 139, 116 mean = 1.39, 0.97
	K	3	GFP	n = 33, 99, 67 mean = 0.07, 0.09, 0.07
		2	Piezo1 – 50 µM	n = 52, 46 mean = 0.58, 0.41
		1	Piezo1 – 100 µM	n = 59 ; mean = 1.01
4	C		siCtrl	n = 239, 104, 69 % = 92.88, 95.19, 86.95
			siPiezo1	n = 210, 108, 66 % = 90.00, 50.00, 80.30
	D	3	siCtrl	n = 222, 99, 60 mean = 1.15, 0.58, 0.73

			siPiezo1	n = 189, 54, 53 mean = 0.74, 0.46, 0.48
	F	3	siCtrl	n = 171, 136, 165 % = 92.39, 92.64, 84.84
			siPiezo1	n total = 193, 198, 222 % = 81.34, 78.39, 83.33
	G	3	siCtrl	n = 157, 166, 124 mean = 0.61, 0.70, 0.61
			siPiezo1	n = 157, 170, 185 mean = 0.57, 0.55, 0.48
	H		siCtrl	n as in G mean = 3.67, 4.15, 5.50
			siPiezo1	n as in G mean = 3.42, 3.01, 4.23
	J	3	GFP	n = 29, 52, 41 mean = 0.12, 0.16, 0.07
			Piezo1	n = 45, 18, 36 mean = 0.31, 0.43, 0.57
	K	3	GFP	n as in J mean = 0.19, 0.20, 0.21
			Piezo1	n as in J mean = 0.16, 0.35, 0.25
5	E	2	Yoda1	n = 246, 227 % = 80.49, 97.36
			Yoda1+apyrase	n = 233, 215 % = 63.24, 96.28

	F	2	Yoda1	n = 198, 221 mean = 0.63, 1.21
			Yoda1+apyrase	n = 159, 207 mean = 0.42, 0. 94
	H	2	10 min	n = 108, 95 mean = 0.49, 0.36
			13 min	n = 59, 29 mean = 0.19, 0.14
6	C	3	Ctrl	n = 166, 129, 95 % = 93.37, 97.67, 89.47
			PBC	n = 251, 155, 143 % = 90.44, 92.25, 60.84
	D	3	Ctrl	n = 157, 127, 85 mean = 0.76, 0.73, 0.45
			PBC	n = 227, 143, 87 mean = 0.51, 0.59, 0.40
	E	3	Ctrl	n as in D mean = 4.12, 4.50, 3.12
			PBC	n as in D mean = 2.91, 3.44, 2.77
	F	3	Ctrl	n = 299, 292, 176 % = 85.28, 91.09, 90.91
			CBX	n = 249, 209, 185 % = 74.69, 42.10, 28.10
	H	3	Yoda1	n = 278, 237, 158 % = 98.50, 92.40, 76.58

			Yoda1+PBC	n = 305, 289, 170 % = 95.73, 90.65, 61.76
	I	3	Yoda1	n = 121, 219, 274 mean = 0.63, 0.59, 1.05
			Yoda1+PBC	n = 105, 262, 292 mean = 0.53, 0.62, 0.72
	K	2	Yoda1	n = 131, 207 mean = 0.64, 0.74
			Yoda1+PBC	n = 68, 115 mean = 0.40, 0.94

Supplemental Figure 1	B	2	DIV 2	n = 456, 632 % of $CK19^+$ cells = 53.42, 50.15
		4	DIV 5	n = 631, 102, 318, 511 % of $CK19^+$ cells = 88.70, 67.51, 72.55, 86.10
		3	DIV 8	n = 602, 788, 951 % of $CK19^+$ cells = 86.53, 69.61, 87.33
		3	DIV 12	n = 73, 81, 577 % of $CK19^+$ cells = 75.06, 15.15, 51.35
	E	2	Krebs	n = 68, 26 mean = 1.14, 1.01
			HYPER	mean = 1.03, 0.99
			ATP	mean = 1.93, 1.74
S2	B	2	DIV 2	n = 297, 342 % of $CK19^+$ ciliated cells = 10.26, 15.15
		4	DIV 5	n = 546, 238, 73, 486

				% of $CK19^+$ ciliated cells = 28.28, 29.32, 22.97, 29.96
		3	DIV 8	n = 534, 606, 731 % of $CK19^+$ ciliated cells = 21.80, 19.72, 19.89
		3	DIV 12	n = 113, 217, 39 % of $CK19^+$ ciliated cells = 21.23, 20, 10.23
	D	3	Ctrl	n = 637, 319, 446 % of $CK19^+$ cells = 80.59, 76.07,86.06
			Chloral hydrate	n = 519, 430, 209 % of $CK19^+$ cells = 92.17, 78.53, 93.49
	E	3	Ctrl	n = 809, 329, 184 % of $CK19^+$ ciliated cells = 26.37, 17.02, 29.89
			Chloral hydrate	n total = 480, 257, 431 % of $CK19^+$ ciliated cells = 12.70, 6.22, 9.28
	G	3	Ctrl	n = 152, 108, 195 % = 51.32, 93.52, 38.97
			Chloral hydrate	n total = 122, 92, 195 % = 63.93, 69.57, 40.00
	H	3	Ctrl	n = 78, 101, 76 mean = 0.51, 0.60, 0.41
			Chloral hydrate	n = 71, 64, 78 mean = 0.43, 0.57, 0.49
	I	3	Ctrl	n as in G mean = 1.08, 1.40, 0.89
			Chloral hydrate	n as in G mean = 0.76, 0.74, 0.60
	K	2	Ctrl	n = 52, 69

				mean = 0.49, 0.58
			Suramin 20 µM	n = 35, 43 mean = 0.60, 0.57
			Suramin 200 µM	n = 16, 22 mean = 0.34, 0.38
S4	B	2	Yoda1	n = 131, 207 mean = 0.64, 0.74
		3	Yoda1+apyrase	n = 109, 136, 53 mean = 0.41, 1.38, 0.75
S6	C	2	Piezo1	n = 21, 15 mean = 0.36, 0.39
			Piezo1 + Panx1	n = 33, 19 mean = 0.58, 0.54
			Piezo1 + Panx1 + P2X4R	n = 41, 34 mean = 0.74, 0.89